

## General Disclaimer

### One or more of the Following Statements may affect this Document

- This document has been reproduced from the best copy furnished by the organizational source. It is being released in the interest of making available as much information as possible.
- This document may contain data, which exceeds the sheet parameters. It was furnished in this condition by the organizational source and is the best copy available.
- This document may contain tone-on-tone or color graphs, charts and/or pictures, which have been reproduced in black and white.
- This document is paginated as submitted by the original source.
- Portions of this document are not fully legible due to the historical nature of some of the material. However, it is the best reproduction available from the original submission.

DOE/JPL-954521-79/9  
DISTRIBUTION CATEGORY UC-63  
IR-10046-2

(DOE/JPL-954521-79/9) INTEGRAL GLASS  
ENCAPSULATION FOR SOLAR ARRAYS Interim  
Report (Spire Corp., Bedford, Mass.) 76 p  
HC A05/MF A01

N79-24452

CSCI 10A

Unclas

G3/44 22157

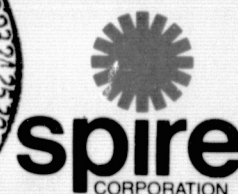
**INTEGRAL GLASS ENCAPSULATION  
FOR SOLAR ARRAYS**

**P.R. YOUNGER  
G.A. LANDIS  
R.G. TOBIN  
W.S. KRISMAN**

**"THE JPL LOW-COST SOLAR ARRAY PROJECT IS  
SPONSORED BY THE U.S. DEPARTMENT OF  
ENERGY AND FORMS PART OF THE SOLAR PHOTO-  
VOLTAIC CONVERSION PROGRAM TO INITIATE A  
MAJOR EFFORT TOWARD THE DEVELOPMENT OF  
LOW-COST SOLAR ARRAYS. THIS WORK WAS  
PERFORMED FOR THE JET PROPULSION LABORATORY,  
CALIFORNIA INSTITUTE OF TECHNOLOGY BY  
AGREEMENT BETWEEN NASA AND DOE."**

**INTERIM REPORT NUMBER 2  
MARCH 1979**

**JET PROPULSION LABORATORY  
CALIFORNIA INSTITUTE OF TECHNOLOGY  
PASADENA, CALIFORNIA 91103**



INTEGRAL GLASS ENCAPSULATION  
FOR SOLAR ARRAYS

Interim Report No. 2

Contract Number 954521

March 1979

Prepared for:  
JET PROPULSION LABORATORY  
California Institute of Technology  
Pasadena, California 91103

Approved by: Peter R. Younger  
Principal Investigator

Approved by: Allen R. Kildpatrick  
Program Manager

SPIRE CORPORATION  
Patriots Park  
Bedford, Massachusetts 01730

## TABLE OF CONTENTS

<u>Section</u>		<u>Page</u>
1	INTRODUCTION . . . . .	1-1
2	PROGRAM PLAN . . . . .	2-1
	2.1 Program Goals . . . . .	2-1
3	TECHNICAL DISCUSSION . . . . .	3-1
	3.1 General . . . . .	3-1
	3.2 Electrostatic Bonding Facility Modifications . . . . .	3-1
	3.3 Glass Development for Electrostatic Bonding . . . . .	3-2
	3.4 Silicon Materials for Electrostatic Bonding . . . . .	3-13
	3.5 Metallization . . . . .	3-17
	3.5.1 Preformed Wire Mesh . . . . .	3-17
	3.5.2 Screen-Printed Metal . . . . .	3-23
	3.6 Module Development . . . . .	3-28
	3.7 Bond Quality Evaluation . . . . .	3-46
	3.7.1 Shear Strength Testing . . . . .	3-46
	3.7.2 Electrostatic Bonding Process Studies . . . . .	3-48
	3.7.3 Empirical Study of Module Bonds . . . . .	3-50
	3.8 Investigation of the Physics of Electrostatic Bonding . . . . .	3-55
	3.9 Economics of Integral Glass Encapsulation . . . . .	3-59
	3.10 Future Development of Integral Glass Encapsulation . . . . .	3-62
4	CONCLUSIONS . . . . .	4-1
	REFERENCES . . . . .	R-1

## LIST OF FIGURES

<u>Figure</u>		<u>Page</u>
3-1	Microprocessor Controlled Electrostatic Bonding Facility . . . . .	3-3
3-2	Process Parameters of a Typical Electrostatic Bond . . . . .	3-4
3-3	Thermal Expansion Characteristics of Corning Glass Compared to Silicon . . . . .	3-6
3-4	Typical Crack Pattern Occurring with Corning 7740 Glass . . . . .	3-7
3-5	Viscosity Curves of Corning Developmental Glasses . . . . .	3-8
3-6	Thermal Expansion of Corning Developmental Glass No. 1 . . . . .	3-9
3-7	Thermal Expansion of Corning Developmental Glass No. 2 . . . . .	3-10
3-8	Thermal Expansion of Corning Developmental Glass No. 3 . . . . .	3-11
3-9	Thermal Expansion of Corning Developmental Glass No. 4 . . . . .	3-12
3-10	GS-328 . . . . .	3-14
3-11	GS-329 . . . . .	3-14
3-12	GS-331 . . . . .	3-15
3-13	GS-327 After Bonding . . . . .	3-16
3-14	GS-327 After Heating to 100°C . . . . .	3-16
3-15	Scanning Electron Micrographs of Textured Silicon Surfaces (1000 x, 60° angle) . . . . .	3-18
3-16	5 x 5 cm Silicon Cell with Wire Screen Front Metallization Electrostatically Bonded to Glass . . . . .	3-19
3-17	AM0 I-V Curve of Cell with Trapped Titanium Coated Silver Screen Metallization . . . . .	3-20
3-18	Configuration for Measuring Contact Resistance Between Bare Cell and Preformed Metal Contact . . . . .	3-24

## LIST OF FIGURES (Continued)

<u>Figure</u>		<u>Page</u>
3-19	Pattern for Testing Screen Printed Metallization and Dielectrics . . . . .	3-24
3-20	AM0 I-V Curve of Cell with Screen Printed Contact Applied to Cover Glass Prior to Bonding . . . . .	3-25
3-21	Cell and Grid Pattern for Testing of Screen-Printed Contacts on Glass . . . . .	3-26
3-22	Bonded Sample with Contacts Screen-Printed on Glass . . . . .	3-26
3-23	AM0 I-V Curve of Cell with Contacts Screen-Printed on Glass . . . . .	3-27
3-24	Four Cell Series Module Type I . . . . .	3-29
3-25	AM0 I-V Curve of Four Cell Electrostatically Bonded Module, Type I . . . . .	3-30
3-26	Four Cell Module with Total Glass Encapsulation, Type II . . . . .	3-31
3-27	AM0 I-V Curve of Four Cell Total Glass Encapsulated Type II Module . . . . .	3-32
3-28	Practical ESB Module Configuration . . . . .	3-33
3-29	Advanced Four-Cell Glass Encapsulated Module . . . . .	3-34
3-30	AM0 I-V Curve of Advanced Four-Cell Glass Encapsulated Module . . . . .	3-35
3-31	Fabrication Sequence for Advanced Type II All Glass ESB Modules . . . . .	3-37
3-32	Integral Module Output Terminal Design . . . . .	3-38
3-33	Combined Electrode and Cell Alignment Fixture for Module Front Bond . . . . .	3-40
3-34	Cell Layout for Incorporation of Six Electrostatically Bonded Assemblies Into One Minimodule . . . . .	3-43
3-35	Cell Layout for Incorporation of Four Electrostatically Bonded Assemblies Into One Minimodule . . . . .	3-44

## LIST OF FIGURES (Concluded)

<u>Figure</u>		<u>Page</u>
3-36	Advanced Bonder Cell Design . . . . .	3-45
3-37	Bond Strength versus Current Limit Set . . . . .	3-51
3-38	Bond Strength versus Bond Voltage . . . . .	3-52
3-39	Bond Strength versus Charge Transfer Setting . . . . .	3-53
3-40	Current and Voltage Characteristics of a Module Front Assembly Bond . . . . .	3-54
3-41	Bond Coverage versus Net Charge Transfer for Module Front Bonds . . . . .	3-56
3-42	Auger Depth Profile of Unbonded Tantalum Film on 7070 Glass . . . . .	3-57
3-43	Auger Depth Profile of Electrostatically Bonded Tantalum Film on 7070 Glass . . . . .	3-58

## LIST OF TABLES

<u>Table</u>		<u>Page</u>
3-1	Properties of Owens-Illinois Glasses . . . . .	3-13
3-2	Results for Cells with Metal Mesh Front Contacts . . . . .	3-21
3-3	Results of Screen-Printed Metallization Experiments . . . . .	3-28
3-4	Results of Attempts to Bond Metal Foils to 7070 Glass . . . . .	3-29
3-5	Summary of Advanced Type II Modules Delivered to JPL . . . . .	3-41
3-6	Preliminary Lap-Shear Test Results . . . . .	3-46
3-7	Average Shear Strength of Antireflective Coatings . . . . .	3-47
3-8	Electrostatic Bonding Parameter Test Schedule . . . . .	3-49
3-9	Corning Glass Works Sheet Glass Development Plan . . . . .	3-60
3-10	Cost Projections for Two Fundamental Designs of ESB Modules . . . . .	3-61



## SECTION 1 INTRODUCTION

This report covers Phase II of a program to develop integral glass encapsulation for solar arrays. Work reported was performed during the period from August 1977 to December 1978. The program objective has been to continue the development of electrostatic bonding (ESB) as an encapsulation technique for terrestrial cells.

Electrostatic bonding is a process with general applicability to joining metals, semiconductors, and insulators to glass without the aid of adhesives. Elevated temperature is employed to produce ionic conductivity within the glass, while an externally applied electric field is used to move mobile ions near the interface being joined, so that permanent chemical bonding can occur. When applied to solar cell encapsulation this technique works well for either bare silicon cells or those with a variety of antireflective coatings.

The advantages of glass as an encapsulant are numerous; optical clarity, moisture impermeability, chemical and environmental stability, and mechanical strength are just a few. Electrostatic bonding takes full advantage of all the favorable properties of glass. No adhesives, potting, secondary encapsulants, sealers, or primers are needed to join the cells to the glass. Furthermore, the bond between the cell and glass is stronger than either material. Thus loss of optical coupling or optical transmission is precluded by the use of electrostatic bonding.

Phase I of this program demonstrated the feasibility of using electrostatic bonding as an encapsulation technique. The current efforts, Phase II, have taken the preliminary module concepts of Phase I and turned these into practical structures that could be scaled up to full size for electric power generating elements. Throughout this program, efforts have been aimed not just at encapsulation processes but at developing whole solar modules produced by electrostatic bonding. Thus such module features as cell interconnections, output terminals, contact metallization, antireflective coating, and mechanical mounting — virtually all parts of a complete system — have been considered and incorporated into the encapsulation process and hardware design.

Economic analyses have shown that this process can be a cost-effective method of producing reliable, long lifetime solar modules. When considered in sufficient volume, both material and equipment costs are competitive with conventional encapsulation systems. In addition, the possibility of integrating cell fabrication into the encapsulation process, as in the case of the preformed cell contacts discussed in this report, offers the potential of significant overall systems cost reduction.

## SECTION 2 PROGRAM PLAN

### 2.1 PROGRAM GOALS

The purpose of this program was to take the demonstrated concepts of electrostatically bonded solar modules and turn them into practical designs incorporating all the features required of a field installed solar array. To accomplish this goal it was necessary to look at equipment and process refinement, materials evaluations, economics of materials and processing, process sequences, environmental testing, bond quality, and module component development. Thus the major tasks of this program were:

- Facility modifications
- Glass development
- Metallization development
- Process studies
- Interconnect and output terminal development
- Bonding of dielectrics
- Module fabrication

Facility modifications were both electrical and mechanical. A microprocessor was to be added for process control. All bonding functions were to be controlled and monitored by this system. Optional manual control was to be available. Throughput was to be increased by the addition of a five sample cassette loading chamber which would eliminate the need for chamber evacuation between each bond. Postbond annealing capabilities were to be available. These modifications were intended to improve process uniformity, improve sample throughput, and extend the range of bonding capabilities.

Glass development was aimed at identifying an optimum glass for the ESB process. Major factors to be considered were applicability to silicon and the glass fabrication processes. Developmental glasses were to be evaluated, while work with glass manufacturers was necessary to define a process and schedule for producing the required glass in quantity and at low cost.

Metallization studies were to be aimed at development of concepts for applying cell contact metal during encapsulation, thus integrating cell processing and module fabrication. Both preformed wire mesh and screen-printed inks on glass were to be evaluated. Both these configurations have potential of providing cell contact and interconnection during encapsulation.

Process studies were intended to determine optimum bond parameters or acceptable ranges of bond parameters. A twofold approach was to be considered. Using the microprocessor control and monitoring system, coupled with a lap shear test setup, a detailed test of bond strength as a function of bond parameters was intended. Meanwhile, various surface analysis techniques such as Auger electron spectroscopy and helium ion backscattering were to be employed in an investigation of the physics of electrostatic bonding.

Development of practical module configurations involved all components of a completed system. Of particular importance were output terminals and interconnections. It was necessary to develop elements that did not compromise the advantages of ESB encapsulation.

The bonding of dielectrics was studied for two applications. First, edge seal materials for double glass modules were needed. Second, bond formation between glass and all potential cell antireflective coatings had to be assessed.

Finally, module fabrication was intended to demonstrate developments throughout the program. Various module configurations and variations were planned.

## SECTION 3 TECHNICAL DISCUSSION

### 3.1 GENERAL

This section will deal with the technical aspects of the program. The accomplishment of the program goals as presented in Section 2 will be discussed in detail. Attention is given to the following areas:

1. Electrostatic bonding facility
2. Glass development for ESB
3. Silicon materials for ESB
4. Metallization development
5. Module development
6. Bond quality evaluation
7. Investigation of the physics of ESB
8. Economics of ESB encapsulation
9. Future development efforts

### 3.2 ELECTROSTATIC BONDING FACILITY MODIFICATIONS

During Phase II, the electrostatic bonder underwent extensive modifications designed to improve the control and reproducibility of the bonding process, to broaden the capabilities of the machine, and to improve sample throughput.

The major bond parameters — time, pressure, voltage, and current — are now simultaneously controlled, logged, and displayed in real time by a Tektronix 4051 microprocessor graphics system. Manual control, by means of 0V-10V control signals, is also possible. The programmable high voltage power supply permits bonding under either constant current or constant voltage conditions or any combination of these, and provides automatic polarity reversal for bi-directional bonding.

Two major modifications were also made to the bonding facility, to enhance its versatility and speed the processing of samples. A system permitting the bonding of five samples in succession, without breaking the bonding environment, has been installed, and has substantially increased throughput. The range of available process variations has

been expanded by the installation of a heated loading table, making possible the application of heat to samples both before and after bonding. Prebond heating permits samples to reach the temperature necessary for glass deformation more quickly, so that the cells are exposed to high temperature degradation for a shorter period of time. Postbond heating slows the cooling of the sample through the annealing range of the glass, so that residual stress in the glass is reduced at room temperature. Such stress can significantly weaken the module structure if cooling is too rapid. The heated loading table provides substantial control of the heat flow to and from the samples, both before and after bonding.

With these additions and modifications, the present electrostatic bonder is a versatile experimental tool. Its features include:

1. Controlled bonding environment, either vacuum or inert gas
2. 8 inch x 8 inch bonding zone
3. Microprocessor control of all bonding functions
4. Real time display and logging of bonding parameters
5. Hard copy of bonding data
6. Programmable high voltage power supply for constant current or constant voltage bonding, and automatic polarity reversal
7. Multiple sample bonding capability
8. Pre-/post-bond sample heating for rapid heating of samples and annealing of glass

A photograph of the facility appears in Figure 3-1. Figure 3-2 shows the parameters of a typical bond, as displayed by the microprocessor graphics unit.

### 3.3 GLASS DEVELOPMENT FOR ELECTROSTATIC BONDING

The ideal glass for electrostatic solar cell encapsulation would have a number of important properties, not all of which are optimized in the Corning 7070 glass currently used. The most important are:

1. Expansion match to silicon at the bonding temperature
2. High optical transmission in the range 0.4 - 1.2  $\mu\text{m}$

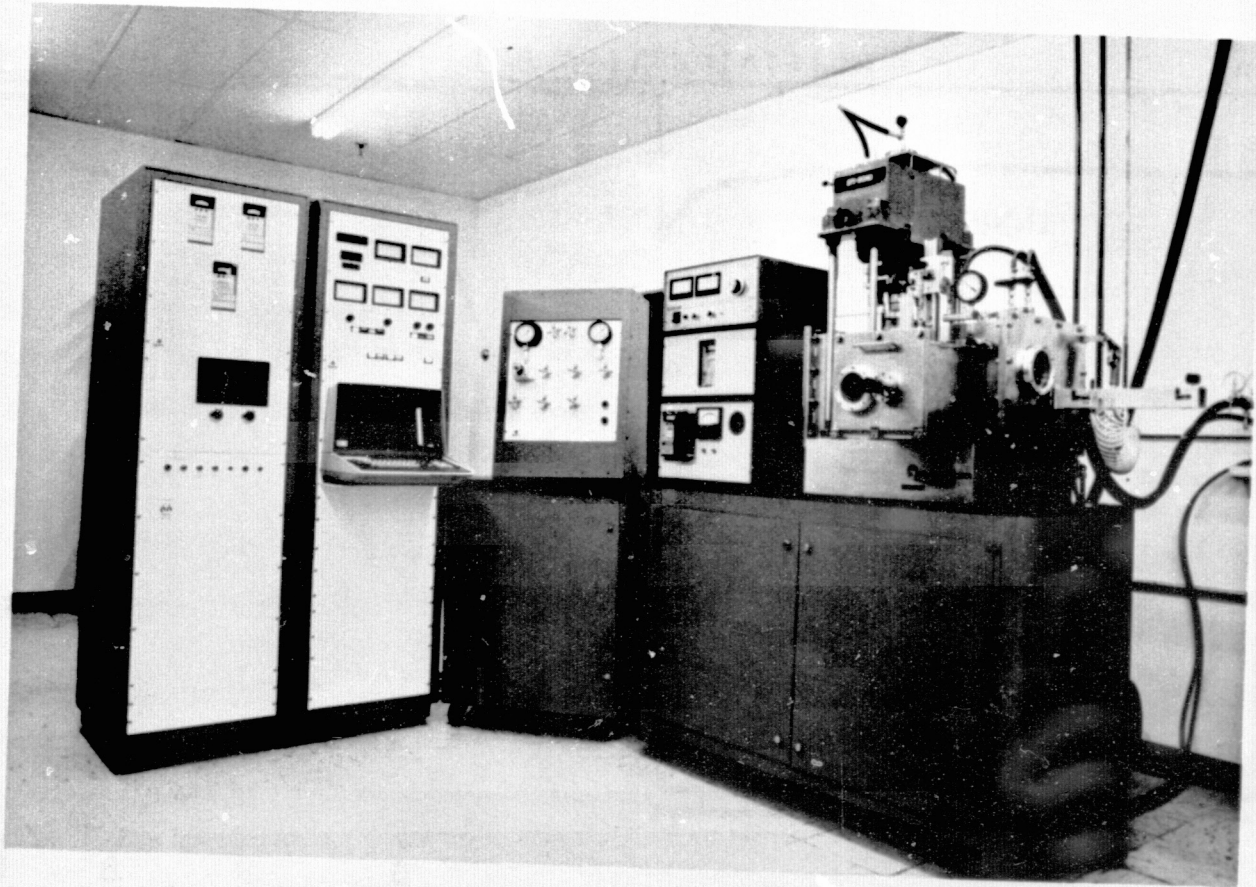


FIGURE 3-1. MICROPROCESSOR CONTROLLED ELECTROSTATIC BONDING FACILITY

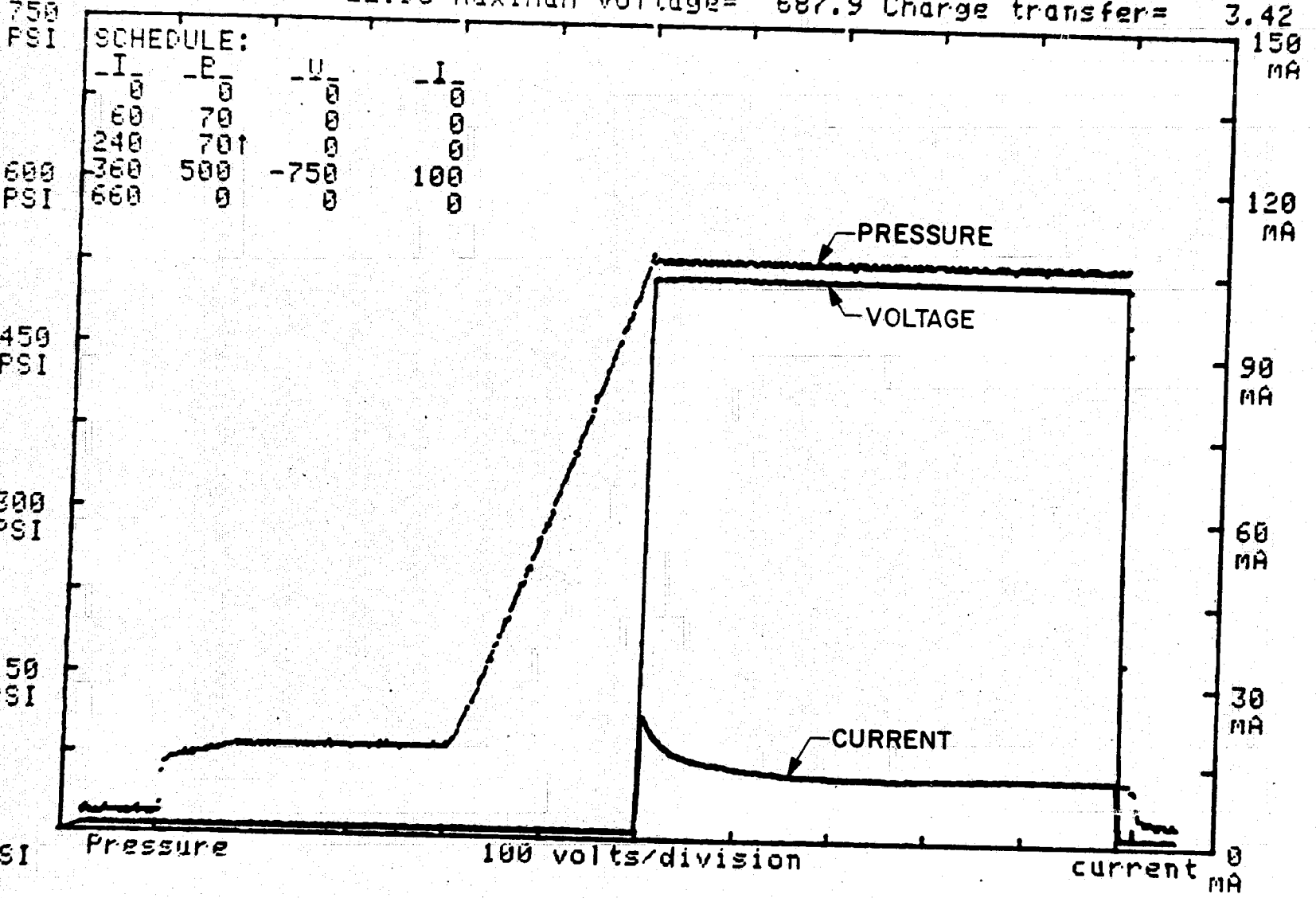
Bond 460-1862 PR

DATE: 375

TIME: 21:46

PRESSURE: initial, 0 PSI FINAL, 500 PSI

Max bond current= 22.95 Maximum voltage= 687.9 Charge transfer= 3.42



3-4

FIGURE 3-2. PROCESS PARAMETERS OF A TYPICAL ELECTROSTATIC BOND



3. Low annealing point
4. No loss of transmission due to environmental exposure

The requirement that the thermal expansion match that of silicon is the most critical one, and is primarily responsible for the choice of Corning 7070. This requirement particularly limits the use of Corning 7740 ("Pyrex"), which is otherwise similar, more resistant to weathering, and more readily available. Figure 3-3 shows the expansion curves for these two glasses and silicon, as well as for window glass. While bonding silicon to 7070 glass at or near the intersection of their expansion curves will result in an essentially unstressed configuration at room temperature, the differential expansion of silicon compared to 7740 results in stresses at room temperature that are beyond the safe working range of the glass. The result is cracking in the glass at the periphery of the bonded region, as shown in Figure 3-4. Such cracking is never seen in 7070 glass. Cracking of 7740 glass could only be eliminated by use of a cell structure that permitted a significantly lower bonding temperature.

Although 7070 is entirely suitable with respect to thermal expansion and optical transmission, its viscosity is rather high, requiring high temperatures for deformation around cell metallization, and its weathering resistance is less than that of 7740 glass. To identify alternatives to 7070 that will improve on these characteristics and still be compatible with silicon bonding, a number of standard and developmental glasses have been tested.

Two commercial glasses equivalent to Corning 7070 — Schott code 8248 and Owens-Illinois ES-1 — have been successfully bonded and subjected to thermal cycling from 100°C to -196°C (the temperature of liquid nitrogen), without delamination or cracking. These glasses appear to be fully suitable for electrostatic bonding of silicon. Another standard glass, Schott Tempax, the equivalent of Corning 7740, was also tried, but behaved much like 7740.

Four developmental glass samples were received from Corning and bonded. The bonds formed with two of the materials were unstable and failed after several days by delamination and cracking of the silicon, indicating that the assemblies were highly stressed and not properly bonded. The other two materials showed similar results, although not all samples failed. None of these materials appears to be fully suitable for

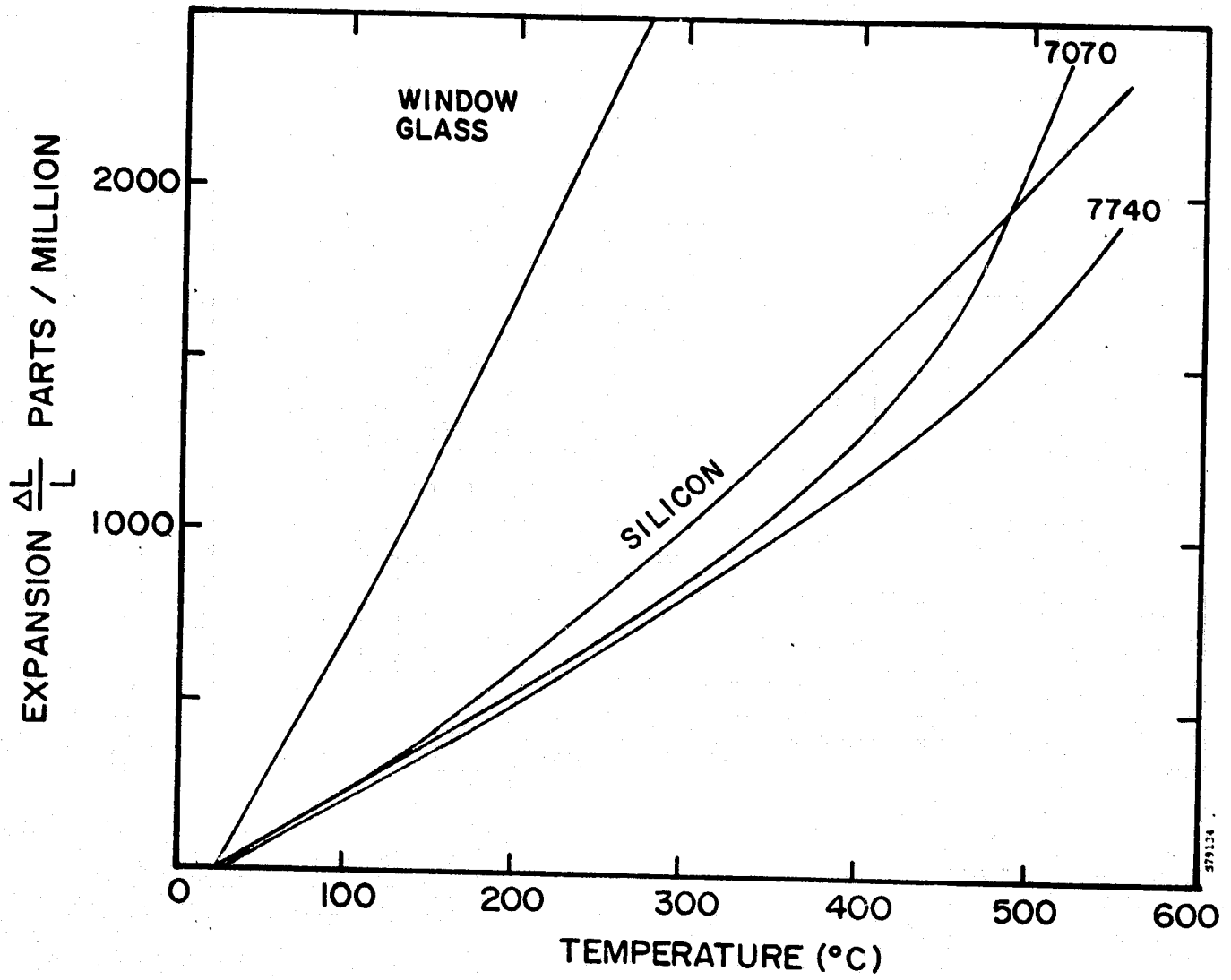


FIGURE 3-3. THERMAL EXPANSION CHARACTERISTICS OF CORNING GLASS COMPARED TO SILICON

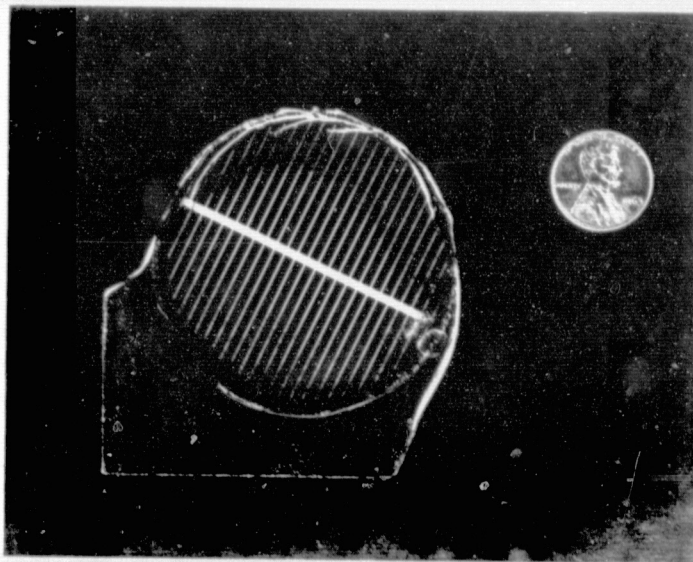


FIGURE 3-4. TYPICAL CRACK PATTERN OCCURRING WITH CORNING 7740 GLASS

electrostatic bonding to silicon. Figure 3-5 shows the viscosity curves of these glasses. Their thermal expansion curves are shown in Figures 3-6, 3-7, 3-8, and 3-9. For reference, the thermal expansion characteristic of silicon is also presented.

In addition to ES-1, seven developmental glasses from Owens-Illinois have been evaluated. Some properties of the Owens-Illinois glasses are listed in Table 3-1. Two of them, GS-210 and GS-332, were extremely hard at the bonding temperature of 600°C, and formed no bonds. Three others — GS-328, GS-329, and GS-331 — bonded well, but broke apart, splintering the silicon, after periods ranging from a few minutes to a few hours at room temperature. Figures 3-10, 3-11, and 3-12 are photographs of these samples, showing the glass cracking and silicon breakup by divoting in the glass. Evidently, these materials do not meet the basic expansion requirements for silicon bonding.

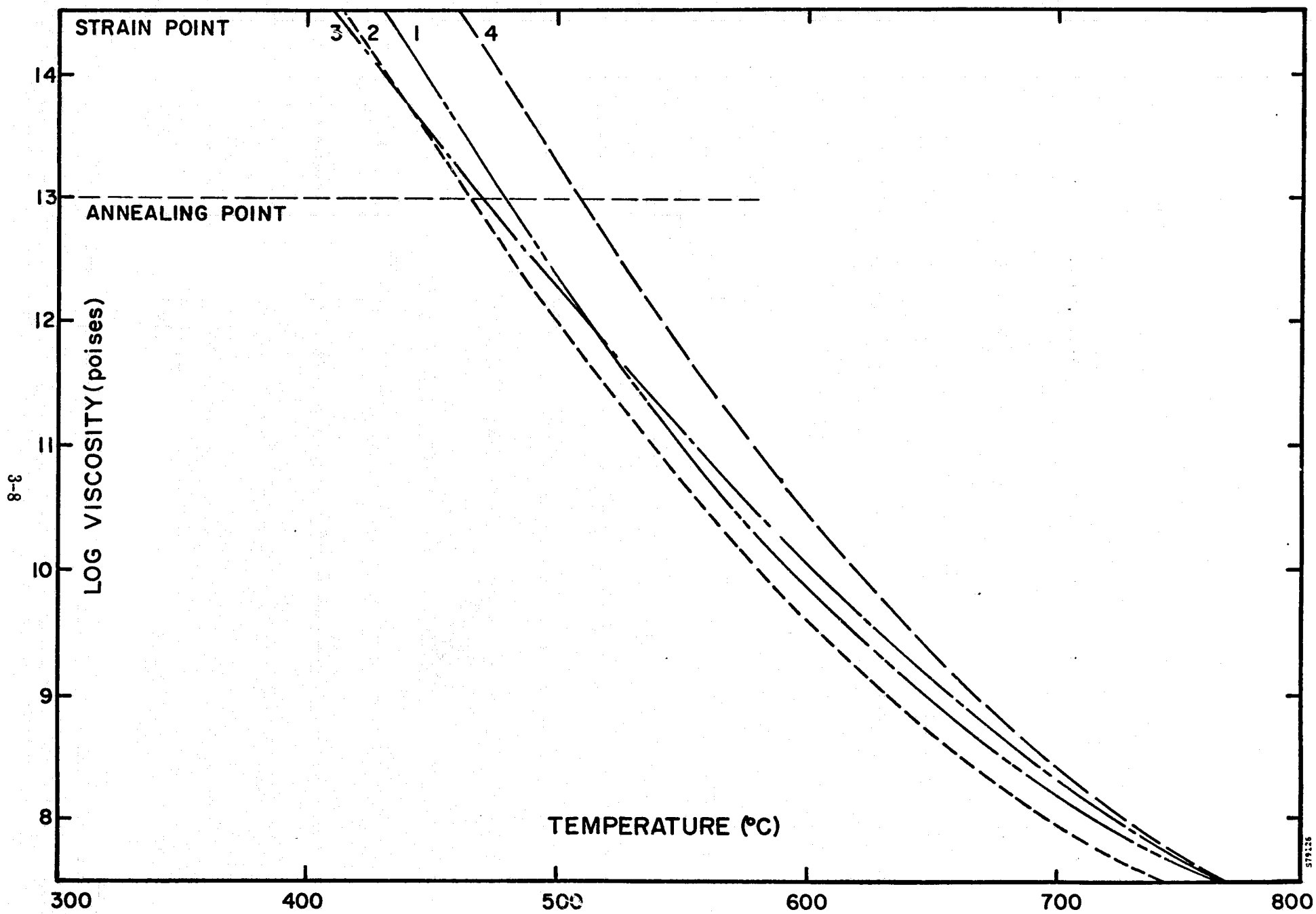


FIGURE 3-5. VISCOSITY CURVES OF CORNING DEVELOPMENTAL GLASSES

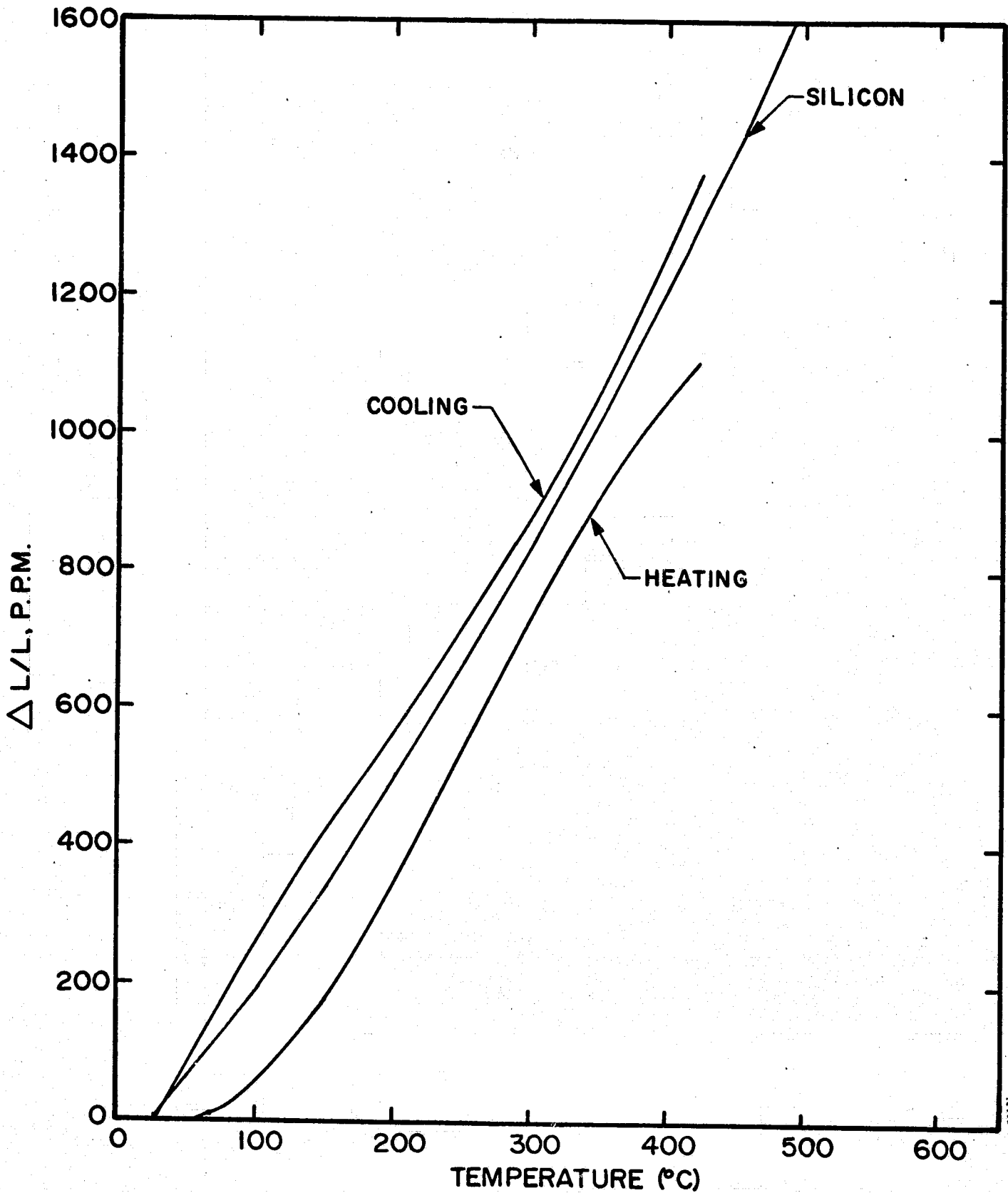


FIGURE 3-6. THERMAL EXPANSION OF CORNING DEVELOPMENTAL GLASS NO. 1

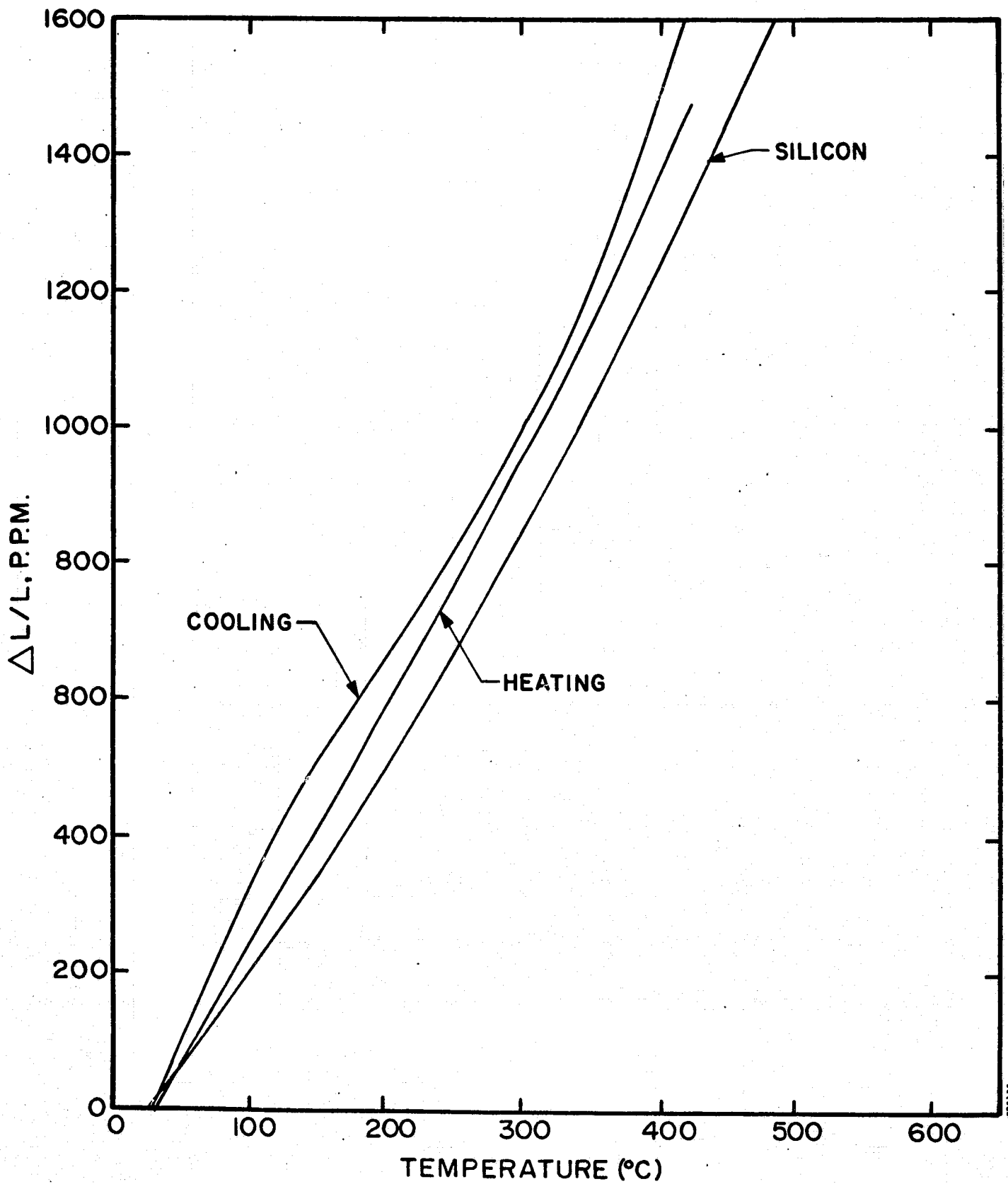


FIGURE 3-7. THERMAL EXPANSION OF CORNING DEVELOPMENTAL GLASS NO. 2

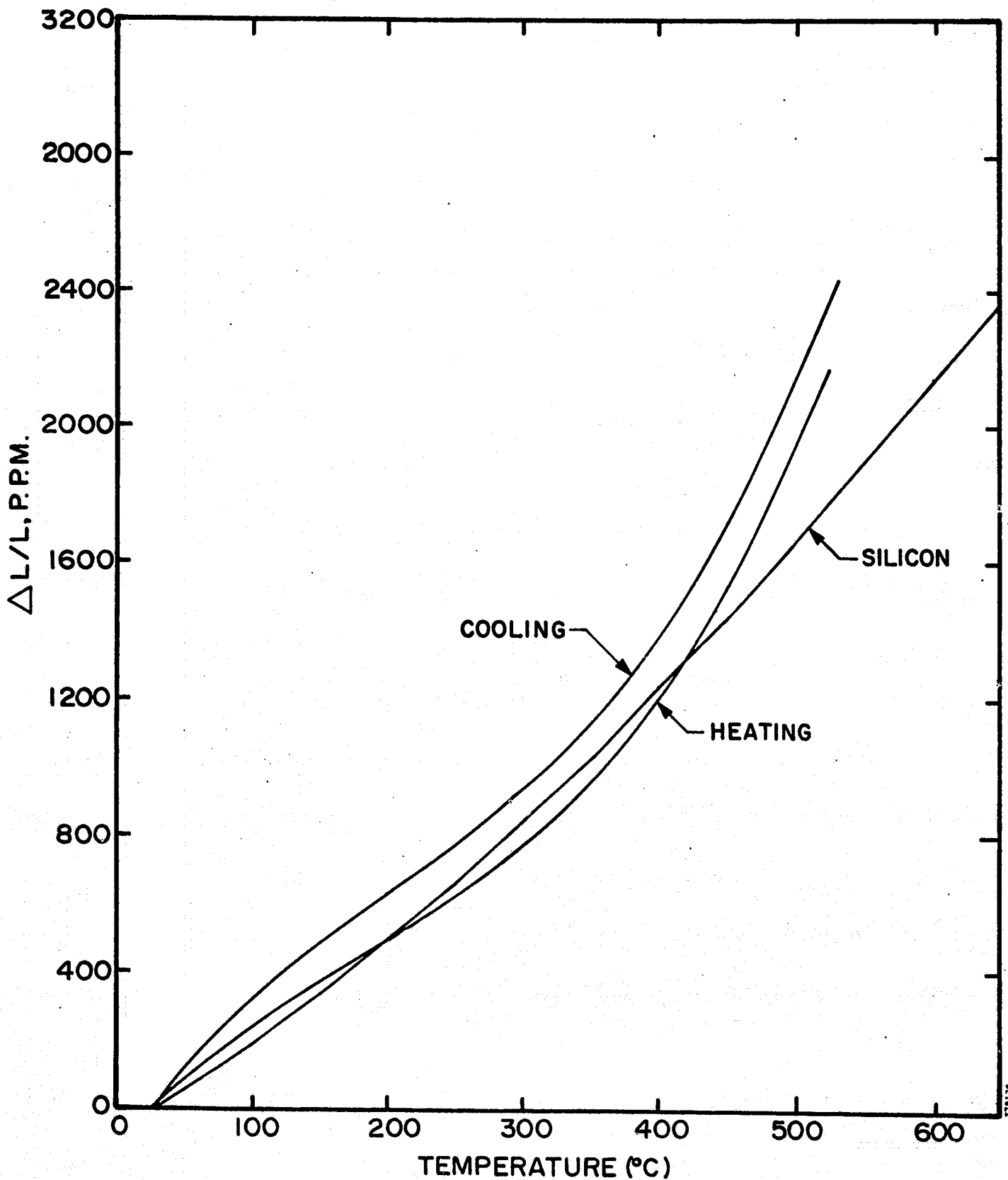


FIGURE 3-8. THERMAL EXPANSION OF CORNING DEVELOPMENTAL GLASS NO. 3

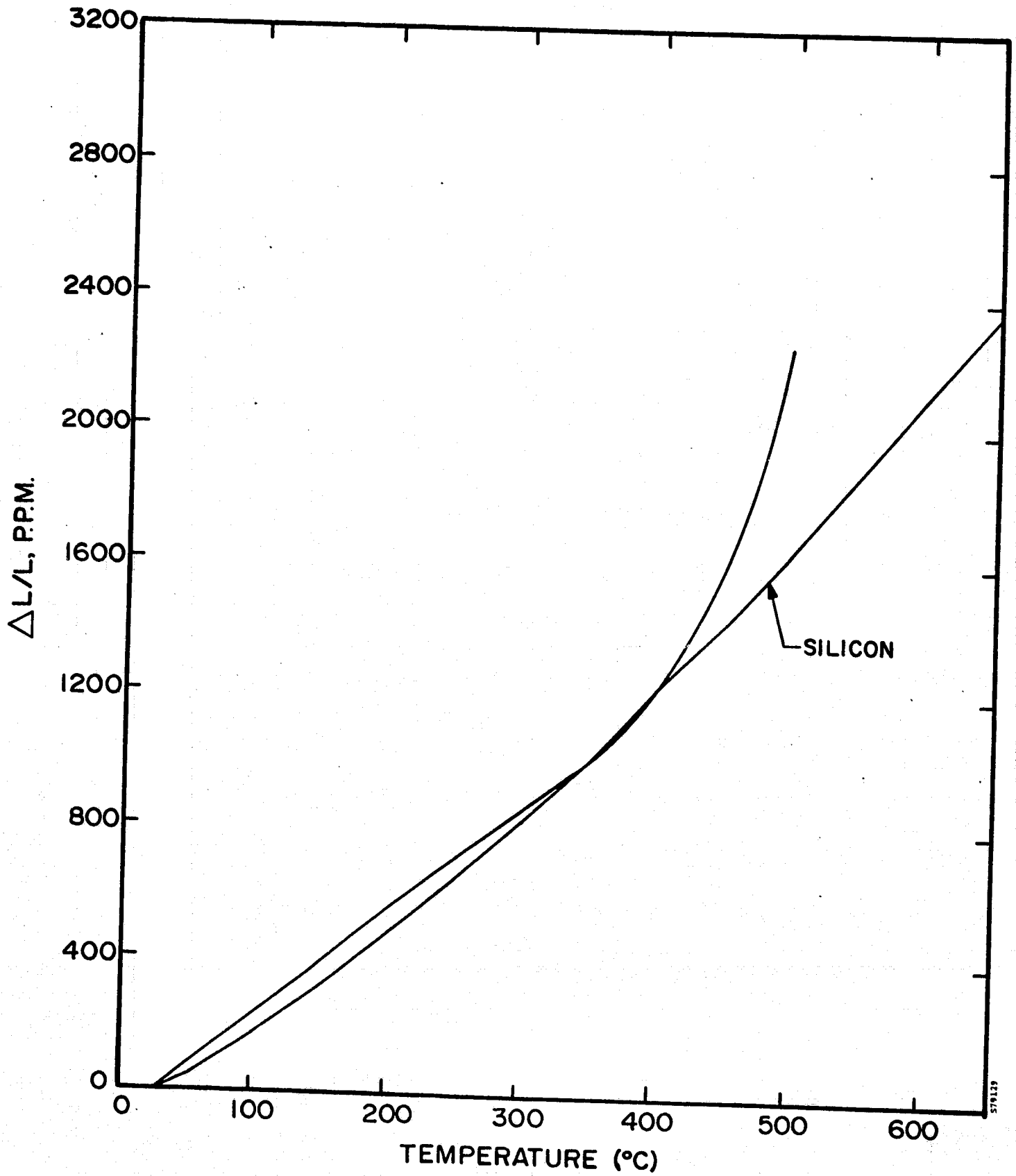


FIGURE 3-9. THERMAL EXPANSION OF CORNING DEVELOPMENTAL GLASS NO. 4



TABLE 3-1. PROPERTIES OF OWENS-ILLINOIS GLASSES

Glass	Softening Point (°C)	Anneal Point (°C)	Strain Point (°C)	Expansion Coefficient (10 <sup>-7</sup> /°C)
ES-1	733	488	450	33.1
GS-327	645	488	456	45.6
GS-328		Similar to GS-327		
GS-329	638	-	-	43.2
GS-210	862	687	636	38.2
GS-330	-	-	-	-
GS-331	685	489	451	41.2
GS-332	-	-	-	-

All data courtesy of Owens-Illinois.

Two other samples -- GS-327 and GS-330 -- were extremely soft at 600°C, and bonded easily. These assemblies were stable at room temperature, but broke up after a few minutes at 100°C. Figure 3-13, a photograph of the GS-327 sample before heating, shows the severe deformation from the initial square shape caused by the wafer and square electrode. Figure 3-14 shows the same sample after heating to 100°C. Such extreme deformation indicated that bonding could occur at a lower temperature, so bonding at 520°C was tried, in the hope of reducing thermal stresses. At that temperature, however, the samples did not bond well, but broke on cooling to room temperature.

### 3.4 SILICON MATERIALS FOR ELECTROSTATIC BONDING

Experiments were conducted during Phase II to determine the bondability of various types of silicon surfaces, including polished, bright-etched, textured, ribbon, and polycrystalline materials. Polished and bright-etched surfaces presented no difficulties, and are routinely bonded. Ribbon silicon successfully bonded at 600°C, under moderate pressure, and the bonding of polycrystalline silicon was also demonstrated.

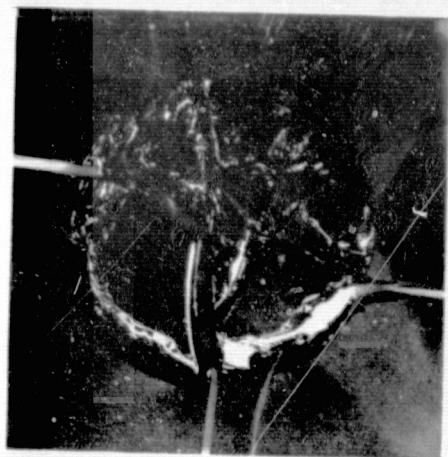


FIGURE 3-10. GS-328

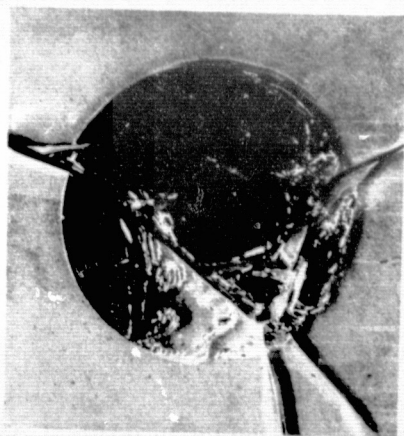


FIGURE 3-11. GS-329

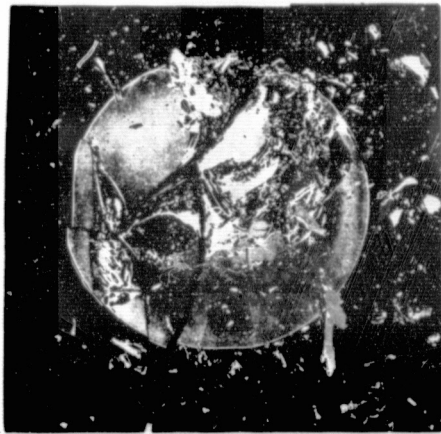
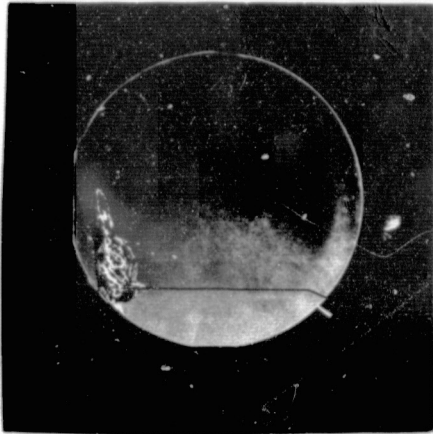


FIGURE 3-12. GS-331

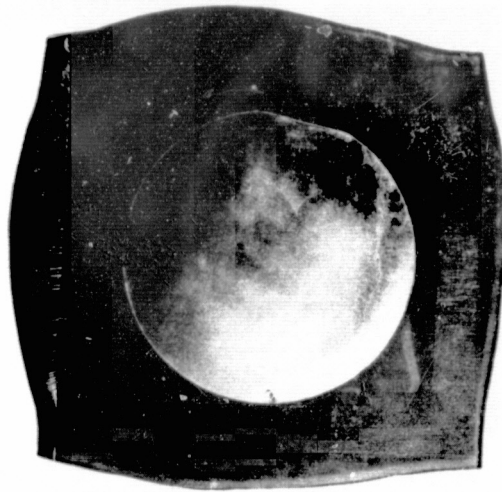


FIGURE 3-13. GS-327 AFTER BONDING



FIGURE 3-14. GS-327 AFTER HEATING TO 100°C

The uneven surfaces of polycrystalline silicon, and particularly of texture-etched silicon, presented a relatively difficult bonding situation, since full deformation of the glass around the irregularities of the surface must be achieved for complete bonding. Such deformation requires a somewhat more severe cycle than is typical for smooth surfaces. Nevertheless, polycrystalline silicon was successfully bonded, and mechanically strong, though still incomplete bonding to the texture-etched surface has been obtained.

The textured silicon used was made by hydrazine etch at Spire Corporation and had an extremely coarse surface by comparison with that used, for example, on HESP (Air Force Contract F33615-75-C-2028) cells. Figure 3-15 shows scanning electron micrographs, at 1000X magnification, of silicon textured at Spire by hydrazine etching and of the surface of a HESP cell formed by NaOH etching. The much finer structure of the HESP cell surface should require less glass deformation, and be correspondingly easier to bond.

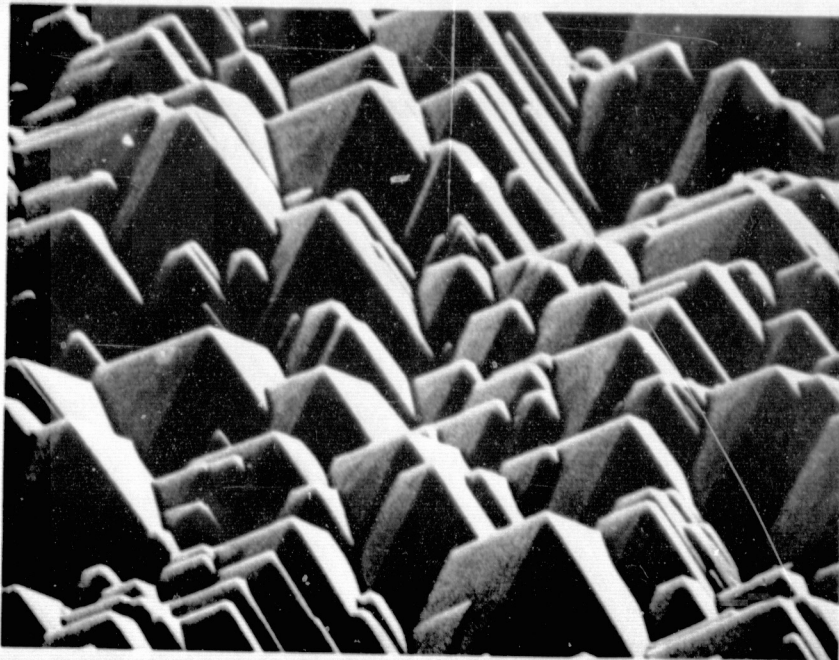
No cells of ribbon, polycrystalline, or textured silicon were bonded, so it is still unknown whether any new problems will arise with active cells of those materials.

### 3.5 METALLIZATION

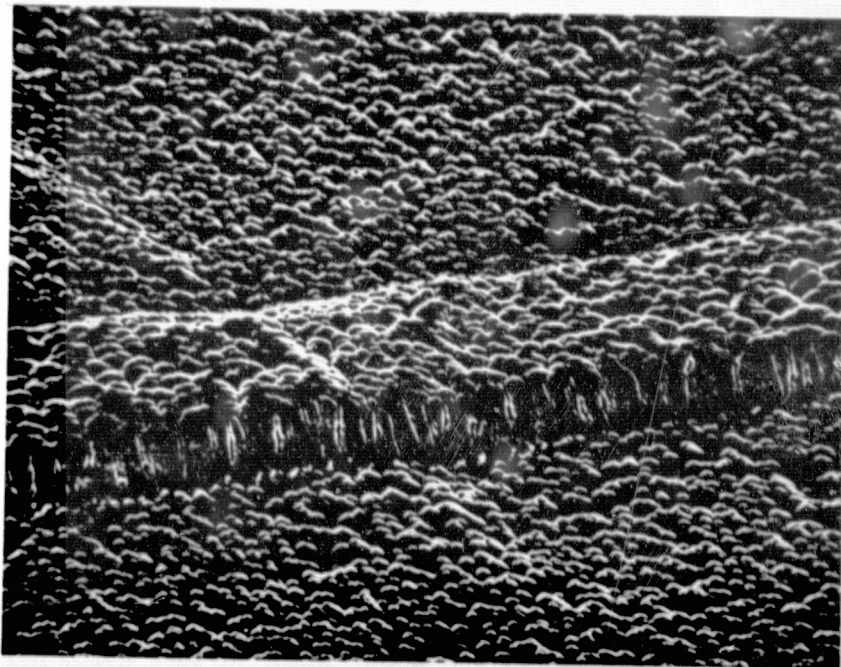
Metallization studies concentrated on inexpensive alternatives to vacuum deposited cell contacts, applied during the electrostatic bonding process. Two configurations investigated were preformed wire mesh, bonded between the cell and the glass, and screen-printed metal applied to the glass before bonding. Both configurations offer the potential advantage of having cell contacts and interconnects applied as an integral unit.

#### 3.5.1 Preformed Wire Mesh

For the preformed wire mesh tests, electroformed meshes were obtained from Buckbee-Mears Corporation. The meshes were made from wire either 48  $\mu\text{m}$  or 14  $\mu\text{m}$  thick, in a pattern of eight lines per centimeter. Silver, nickel, and copper meshes were tried with a variety of overcoatings. The meshes were bonded to 5 cm square cells with no front metallization. Figure 3-16 shows a bonded cell with wire mesh front contact, while Figure 3-17 shows the I-V curve of this cell. The best results are shown in Table 3-2. As the data indicate, good results were obtained with silver mesh, but the best results were seen with silver coated with 1000A of evaporated titanium, and with



Spire etched  
silicon



HESP cell

FIGURE 3-15. SCANNING ELECTRON MICROGRAPHS OF TEXTURED SILICON SURFACES (1000 x, 60° angle)

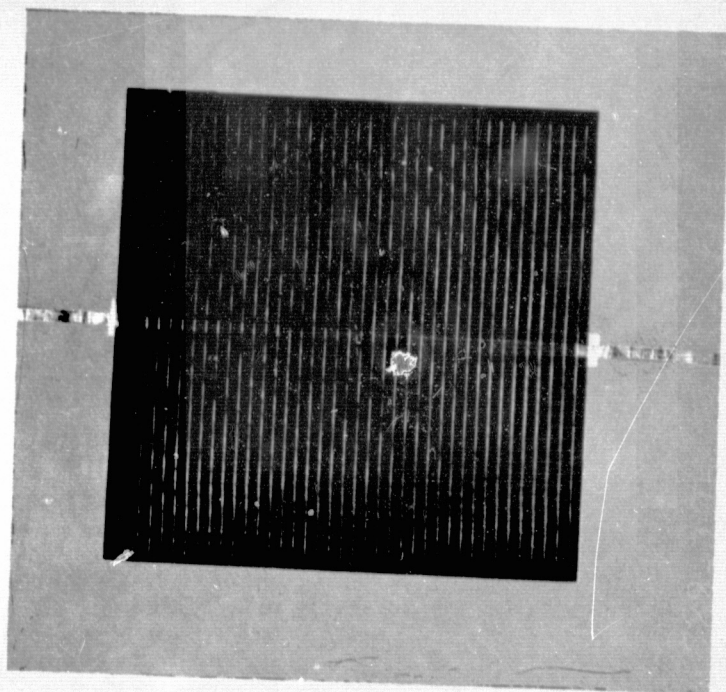


FIGURE 3-16. 5 x 5 cm SILICON CELL WITH WIRE SCREEN FRONT METALLIZATION ELECTROSTATICALLY BONDED TO GLASS

pure silver mesh bonded to a wafer dipped in buffered hydrofluoric acid to remove oxide immediately before the bond. Copper and nickel produced poor results, probably due to cell shunting by metal diffusion into the junction.

Other meshes tested were woven Monel mesh and expanded silver mesh. Both proved difficult to bond due to the major deformation (several mils) needed. Both also had poor results, in many cases fracturing the cells.

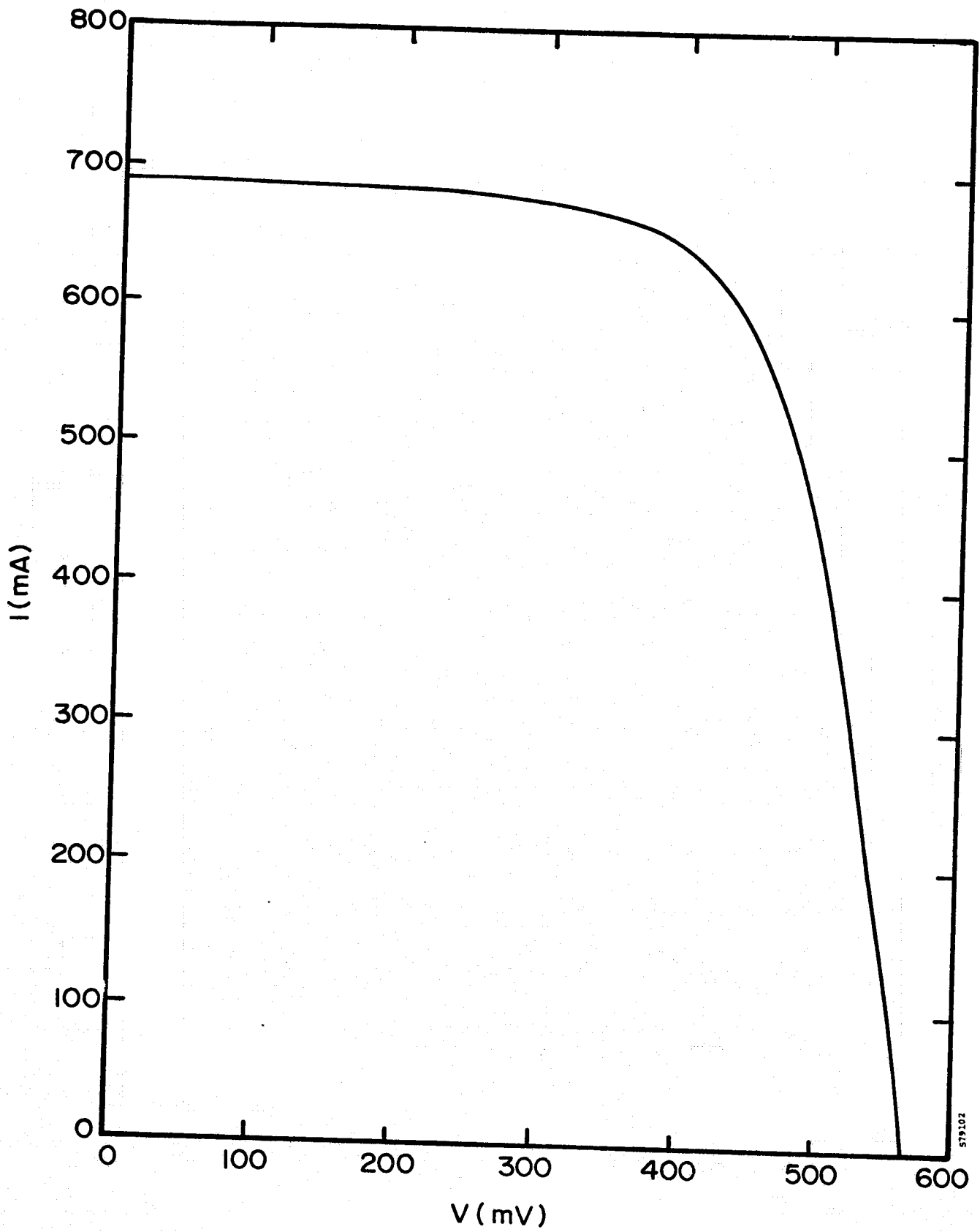


FIGURE 3-17. AM0 I-V CURVE OF CELL WITH TRAPPED TITANIUM COATED SILVER SCREEN METALLIZATION



TABLE 3-2. RESULTS FOR CELLS WITH METAL MESH FRONT CONTACTS (AM0 ILLUMINATION)

Mesh	Line Spacing (lines/cm)	Line Thickness ( $\mu\text{m}$ )	$I_{sc}$ (mA)	$V_{oc}$ (mV)	$P_m$ (mW)	CFF (%)
Silver	8	48	590	575	225	66
Silver	8	14	721	564	216	53
Silver/Titanium	8	48	688	563	263	68
Copper	8	48	500	150	21	28
Copper/Silver	8	48	142	471	19	29
Nickel	8	14	675	122	25	30
Nickel/Titanium	8	48	240	80	5	26
Tungsten	16	25	604	460	146	53
Silver (cell w/HF dip)	8	48	570	570	225	69

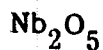
The cells produced to date have no antireflection (AR) coating. Approximately 10 percent improvement in short-circuit current is expected if a technique to lower reflectance can be used on the cell. An additional gain of up to 4 percent could be realized if the glass/air interface reflectance could be lowered by means of an AR coating. There are three possible methods of lowering reflection:

1. Applying an AR coating to the cell prior to bonding
2. Applying an AR coating to the glass side of the interface prior to bonding
3. Texturizing the silicon surface

Applying an AR coating to the cell would ordinarily prevent the establishment of a low resistance contact between the preformed metallization and the wafer. This could be avoided by patterning the coating to leave bare the places to be covered by mesh,

making the AR coating conductive, or having the metal mesh react with the AR coating during bonding. An alternate procedure would be to deposit a fine-line metal pattern, only a few hundred to a few thousand angstroms thick, before plasma depositing a coating of silicon nitride. Exposed silver is not coated by this process and thus would permit the main conductor to carry current from the cell.

The second possibility requires the ability to bond bare silicon to AR coated glass. To test this possibility, silicon bonding was attempted with the following dielectric oxides applied in 700A layers to 7070 glass:



Of these,  $\text{Al}_2\text{O}_3$ ,  $\text{Ta}_2\text{O}_5$ , and  $\text{ZrO}_2$  bonded successfully, surviving cycling from  $-196^\circ\text{C}$  to  $+100^\circ\text{C}$  without failure. The other samples failed to bond at all. The indices of refraction (depending on deposition conditions) of the successfully bonded substances in thin films are<sup>(1-5)</sup>:



Tantalum pentoxide is an excellent AR coating and is currently in standard use on solar cells.

Although not yet attempted with wire mesh contacts, the results of bonding to texturized silicon are reported in Section 3.4.

Contact resistance on a wire mesh sample was measured using the test setup of Figure 3-18. Measured contact resistance was between 20 and 30 milliohm-cm<sup>2</sup>, a value which accounts for a reduction of approximately 2 percent in cell fill factor.

### 3.5.2 Screen-Printed Metal

Applying metal by bonding glass along with screen-printed metal to a bare cell has also been investigated. Figure 3-19 shows the screened test pattern used. In most tests, the module edge seal was tested separately. Initial tests on bare cells used three silver inks from Owens-Illinois, Inc. and Thick Film Systems. All the cells bonded had poor fill factors, attributable largely, but not completely, to series resistance. Figure 3-20 is the I-V curve of a cell with this screened metal as the only front contact. A separate test was tried with the same inks, using a short HF dip before bond for the cover glasses, to etch away glass frit on the surface of the metal. The dip had little effect.

An additional set of screen-printed ink experiments was tried with fine metallization applied to the cell before bond, to reduce contact resistance. Figure 3-21 shows this test setup. Test runs were conducted on four silver inks, processed at three firing temperatures each. Figure 3-22 is a photograph of a typical sample, while Figure 3-23 shows the I-V curve from this sample. Twenty-four samples in all were bonded, with the best cell curve factors produced being on the order of 70-72 percent. Results are shown in Table 3-3. None of the inks proved markedly superior to any of the others.

Cells processed in this manner, if made with the contact metal of the cell indexed to register completely with the silkscreened lines on the glass, show the potential for efficiencies comparable to those of other cells with screen-printed contacts on the silicon. Efficiencies are limited by the resistivity of the screened lines and the minimum line width. Resistivity of around twice the bulk resistivity of the metal and minimum line widths of 250 micrometers are typical. It is possible that resistivity may be decreased, since longer firing schedules may be used when firing ink on glass, where there is no danger of shunting the solar cell junction during firing. The advantage of this system would be single step attachment of parallel interconnects between cells in a module.

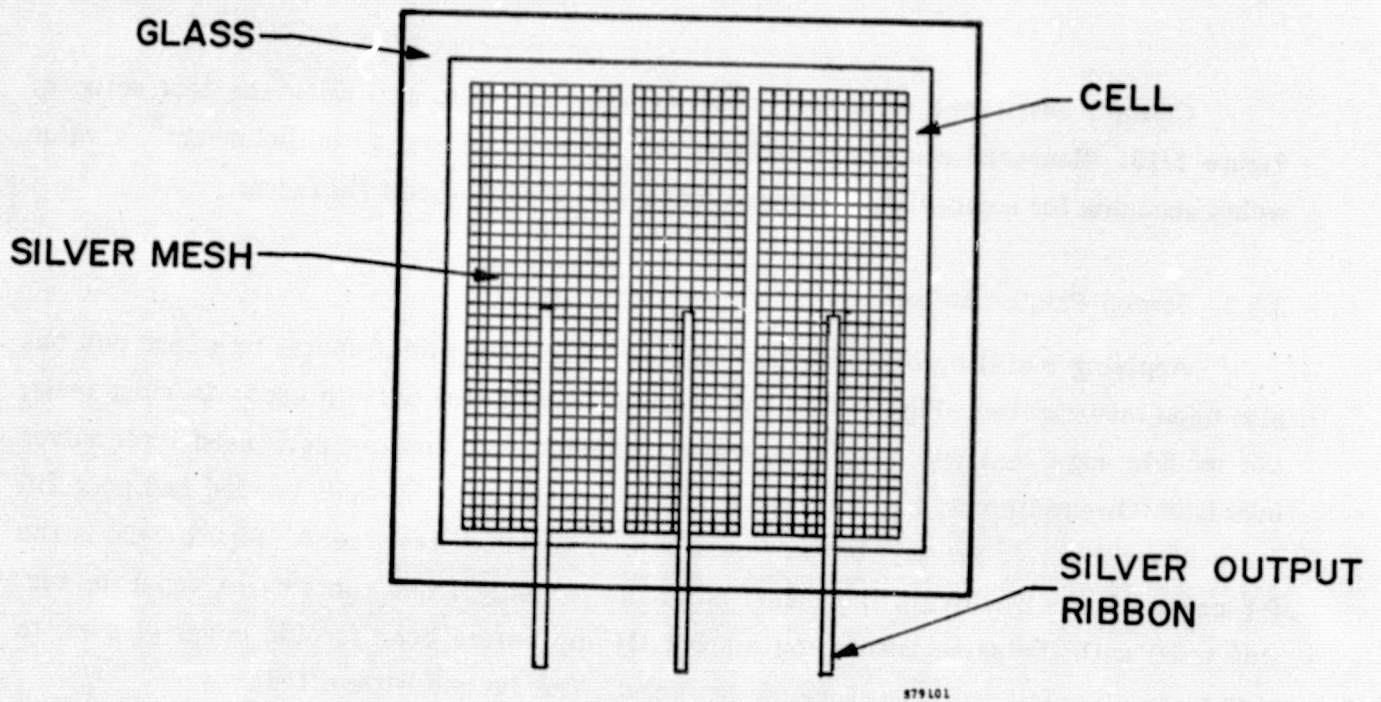


FIGURE 3-18. CONFIGURATION FOR MEASURING CONTACT RESISTANCE BETWEEN BARE CELL AND PREFORMED METAL CONTACT

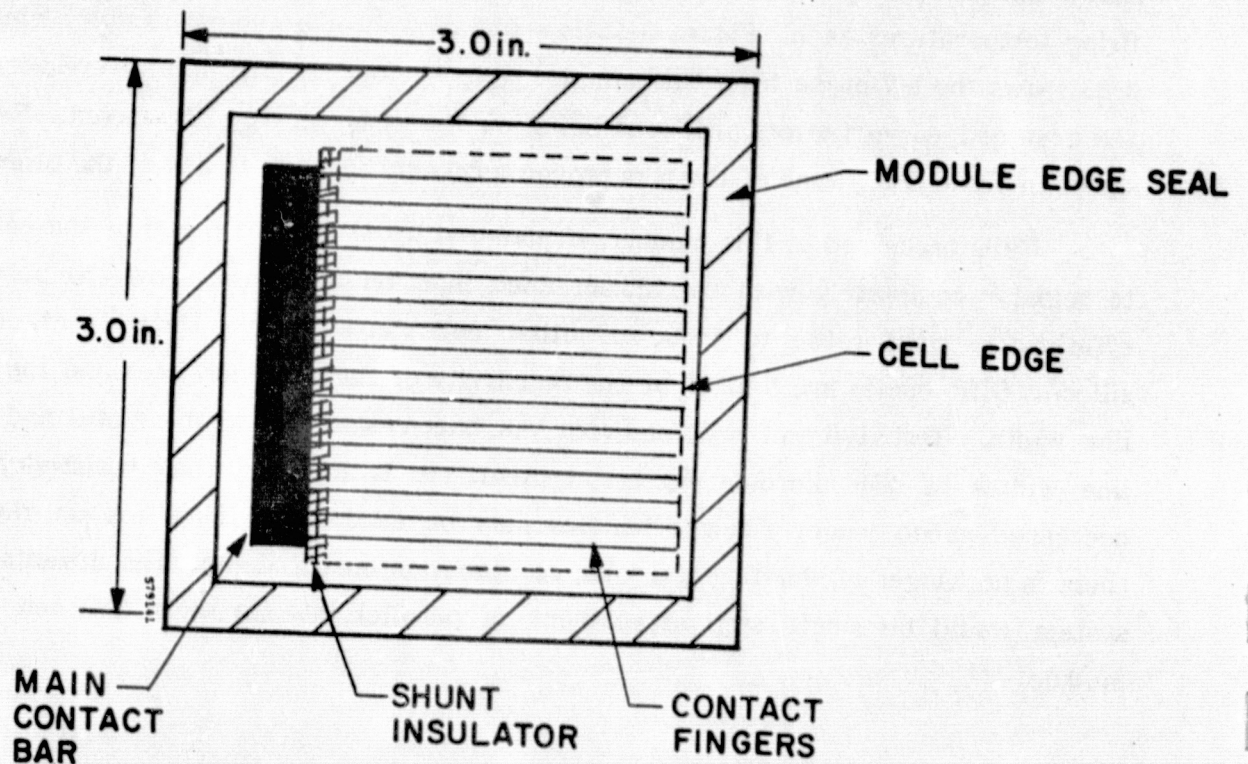


FIGURE 3-19. PATTERN FOR TESTING SCREEN PRINTED METALLIZATION AND DIELECTRICS

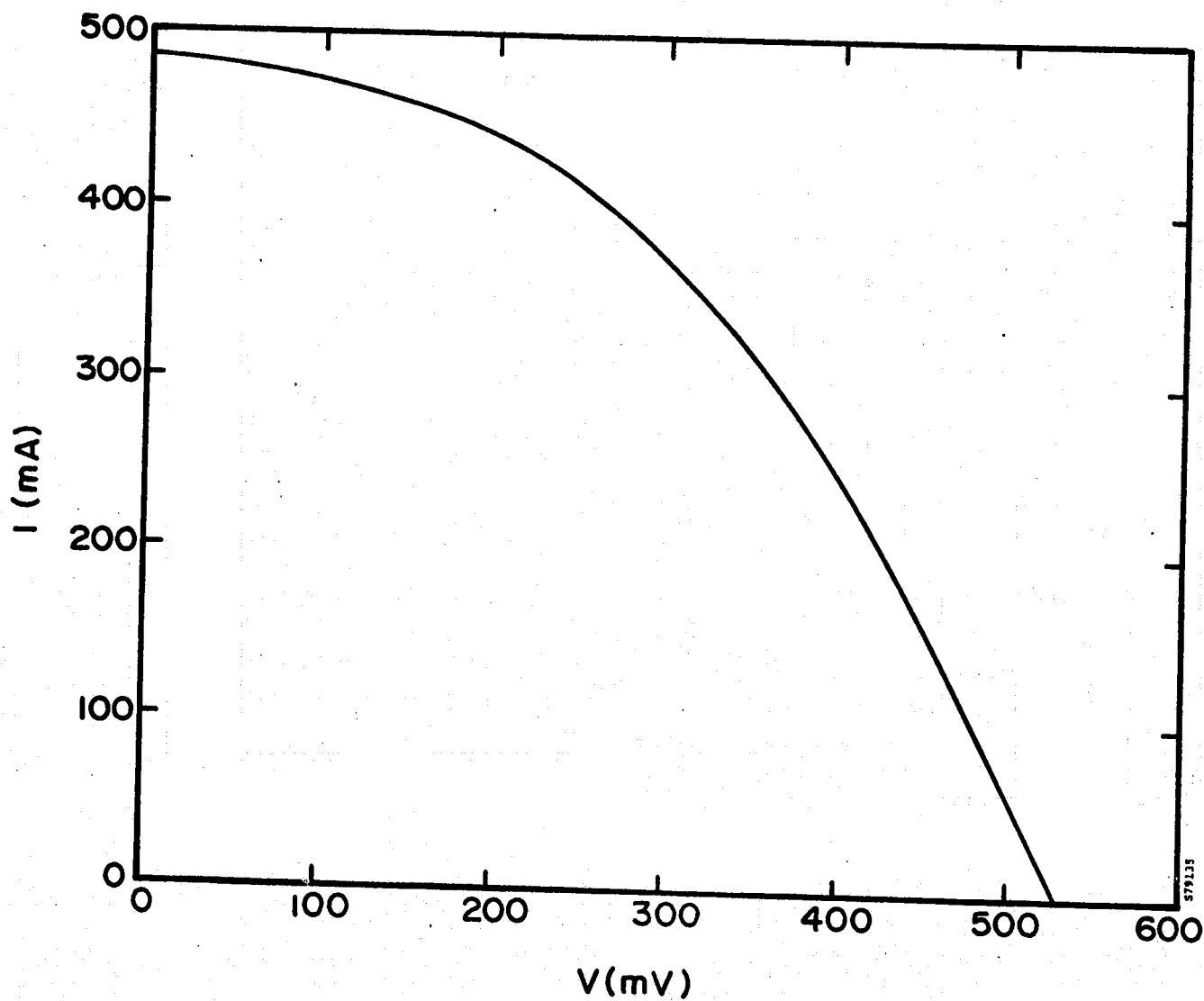


FIGURE 3-20. AM0 I-V CURVE OF CELL WITH SCREEN PRINTED CONTACT APPLIED TO COVER GLASS PRIOR TO BONDING

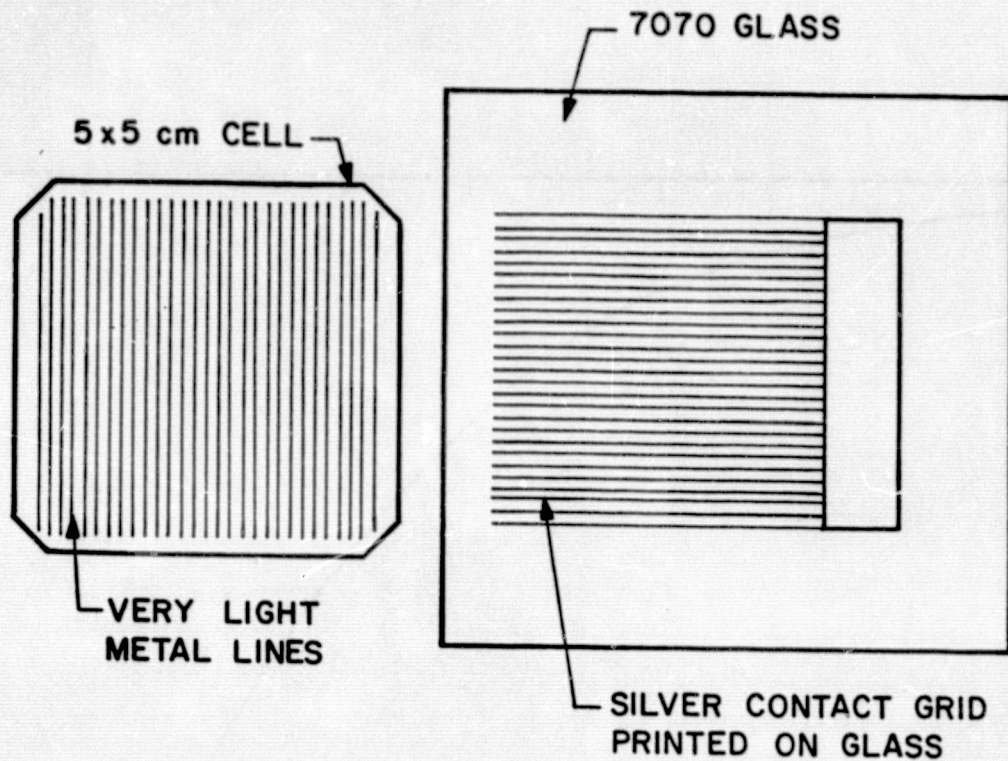


FIGURE 3-21. CELL AND GRID PATTERN FOR TESTING OF SCREEN-PRINTED CONTACTS ON GLASS

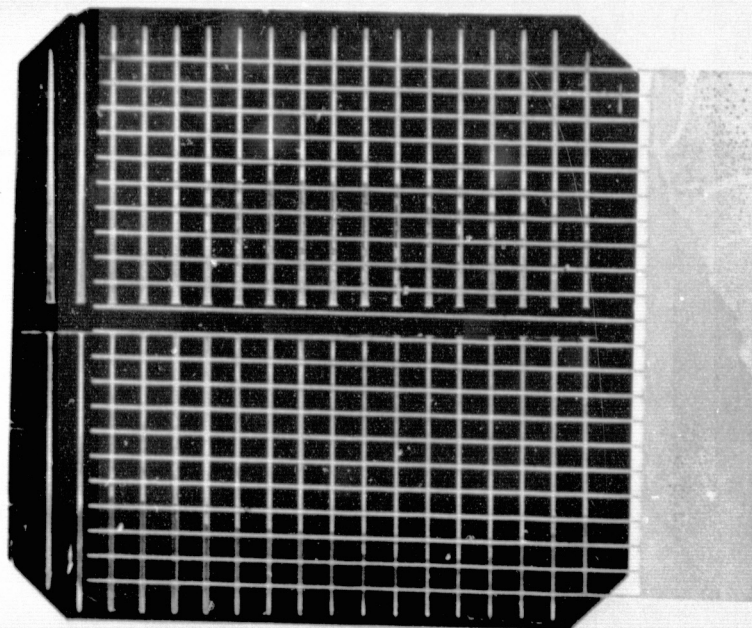


FIGURE 3-22. BONDED SAMPLE WITH CONTACTS SCREEN-PRINTED ON GLASS

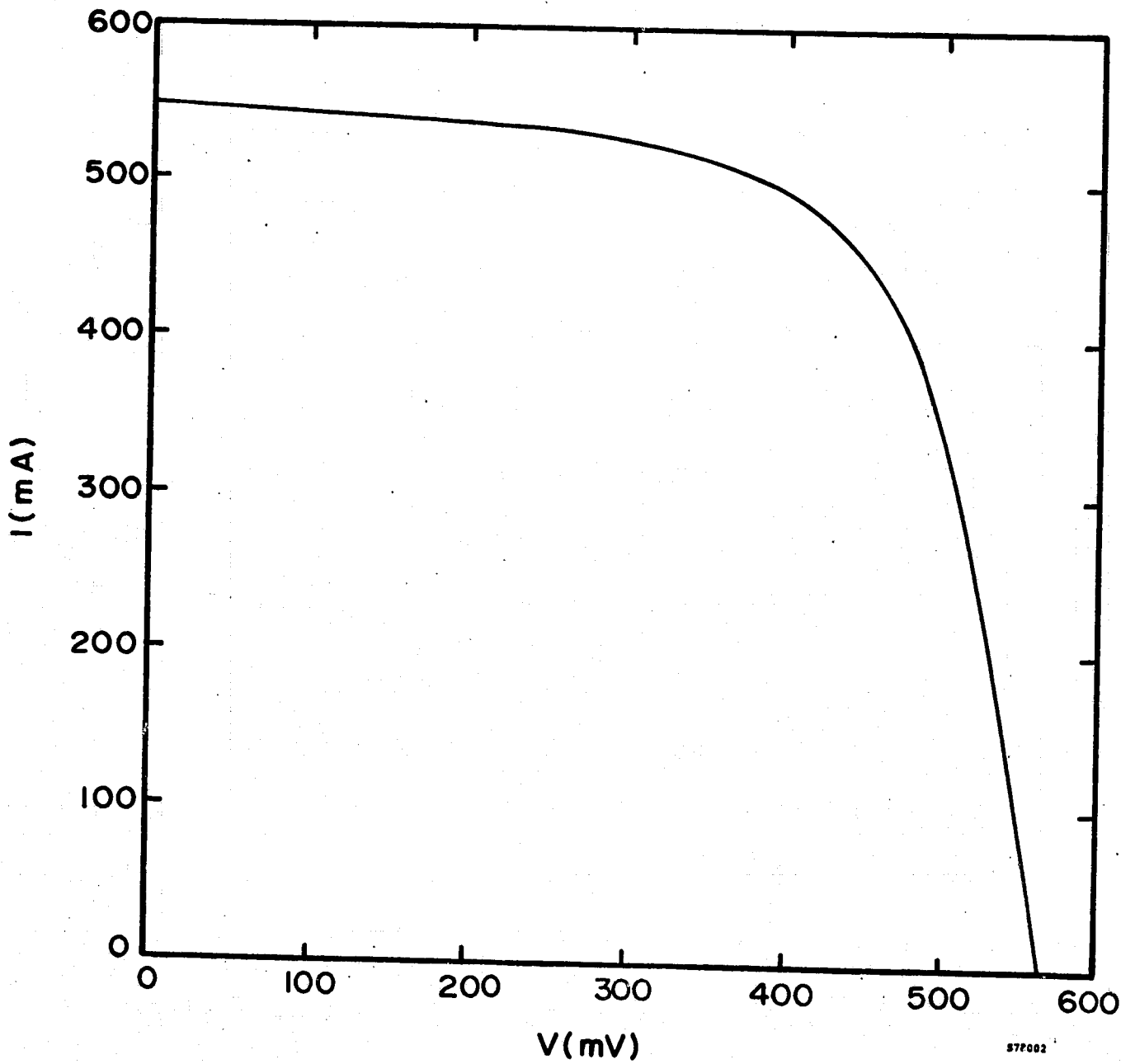


FIGURE 3-23. AM0 I-V CURVE OF CELL WITH CONTACTS  
SCREEN-PRINTED ON GLASS

TABLE 3-3. RESULTS OF SCREEN-PRINTED METALLIZATION EXPERIMENTS

Ink	Firing Temperature (°C)	Average	
		P <sub>max</sub> (mW)	CFF (%)
TFS-A250 (pure silver)	480	153	67.0
	600	116	64.0
	750	203	66.5
TFS-3345 (silver w/frit)	480	180	72.0
	600	135	65.5
	750	175	68.6
TFS-3347	480	177	65.2
	600	180	67.3
	750	161	67.1
OI 6103	575	155	58.4
	650	110	65.0
	750	170	68.7

### 3.6 MODULE DEVELOPMENT

During Phase I of this program, two basic types of demonstration modules were developed and demonstrated. Type I was a four-cell, integral-front module, consisting of four circular cells electrostatically bonded to a single sheet of glass. An evaporated film of titanium-silver surrounding each cell brought current out from the front, and soldered silver mesh provided series interconnections. The back of the module was protected by an organic coating, consisting of an RTV sealant or an asphalt/butyl rubber compound. A photograph and I-V curve of such a module are presented in Figures 3-24 and 3-25.

Total glass encapsulation was demonstrated with the fabrication of Type II modules. Sealing of the back was accomplished by the electrostatic bonding of a second glass piece, using an intermediate dielectric film as a bonding medium. A shallow recess was machined in the back glass to accommodate the cells and interconnections. The use



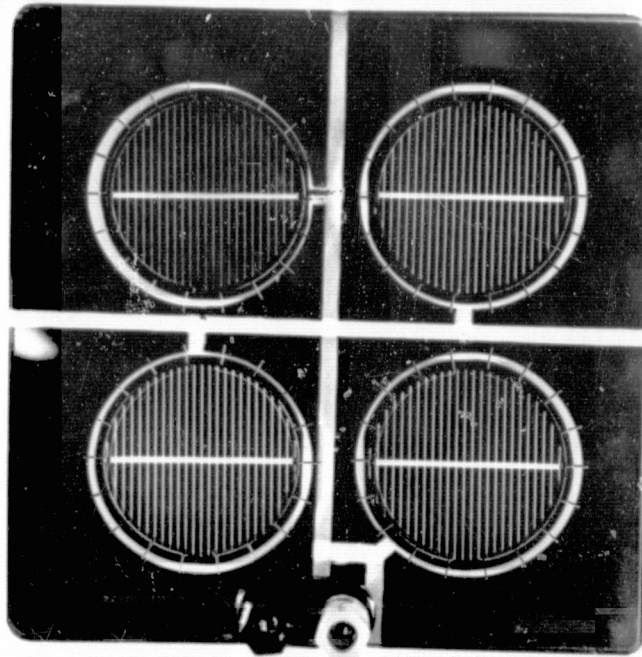


FIGURE 3-24. FOUR CELL SERIES MODULE TYPE I

of evaporated metal films for interconnections was abandoned in favor of more practical welded silver ribbon. Aluminum foil pads, bonded to an extension of the front glass, provided the basis for the attachment of output terminals. A photograph and I-V characteristic are presented in Figures 3-26 and 3-27.

Neither of these designs was intended to represent a practical large-scale array component. They served, however, to demonstrate the feasibility of electrostatic bonding, provide a baseline for evaluation of various components of module design, and produce test samples for JPL. All modules of both basic configurations survived LSA acceptance testing without electrical or mechanical failure of any sort.

Phase II has seen considerable advancement in the design of both module types, with the aim of demonstrating all of the components of a practical module production process. Both types are based on an integral front glass assembly consisting of four 5 cm x 5 cm square cells electrostatically bonded to a single piece of glass, and connected in series by means of welded silver ribbons. The fabrication of modules with square cells demonstrates the compatibility of ESB with the high packing densities required for practical, large-scale arrays.

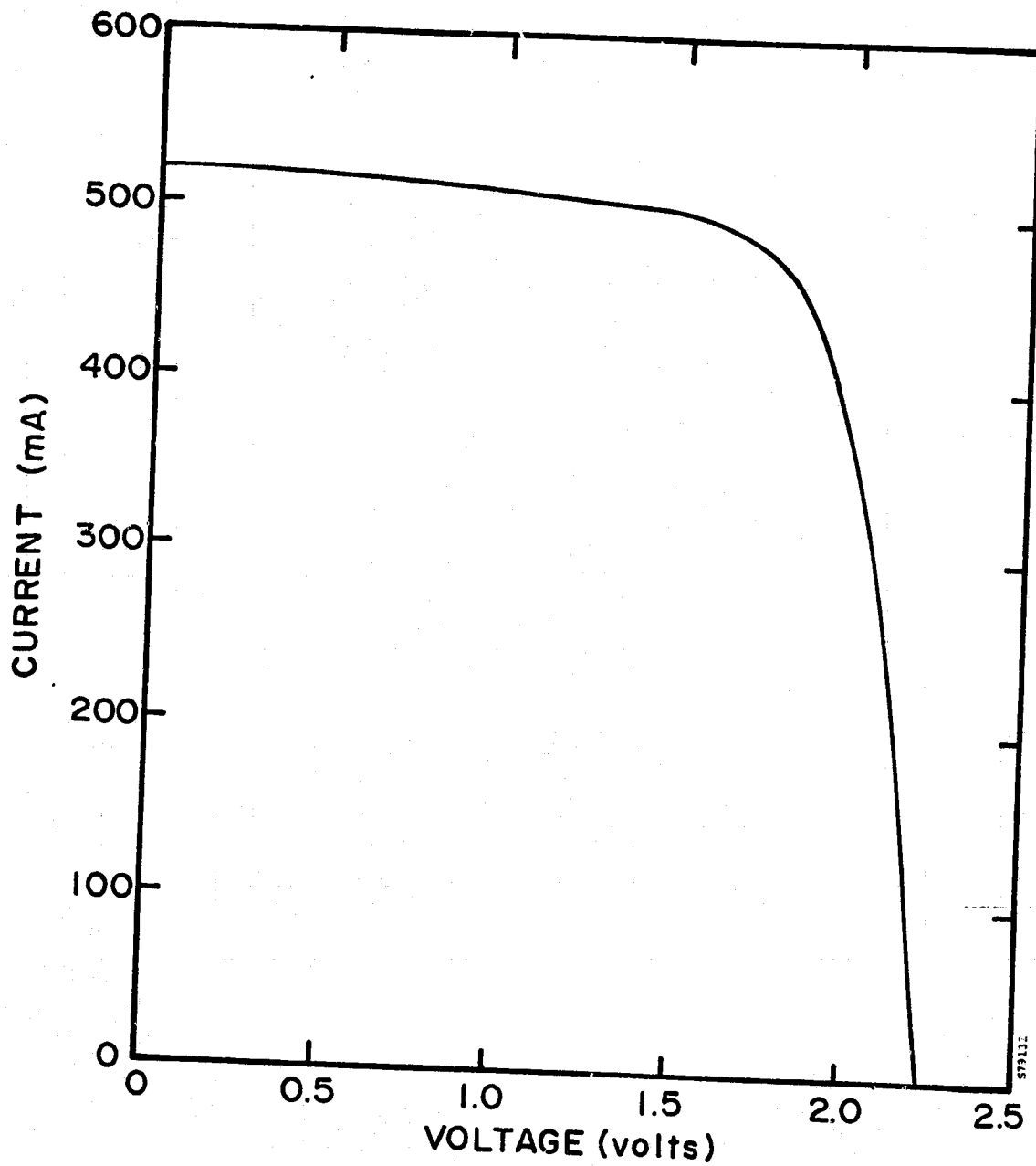


FIGURE 3-25. AM0 I-V CURVE OF FOUR CELL ELECTROSTATICALLY BONDED MODULE, TYPE I

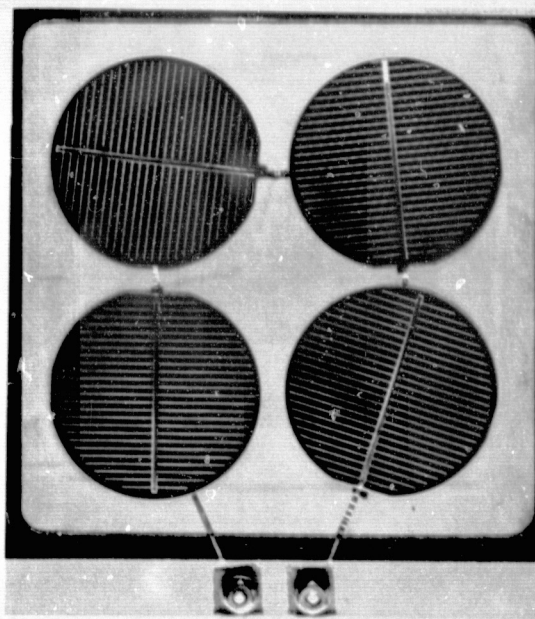
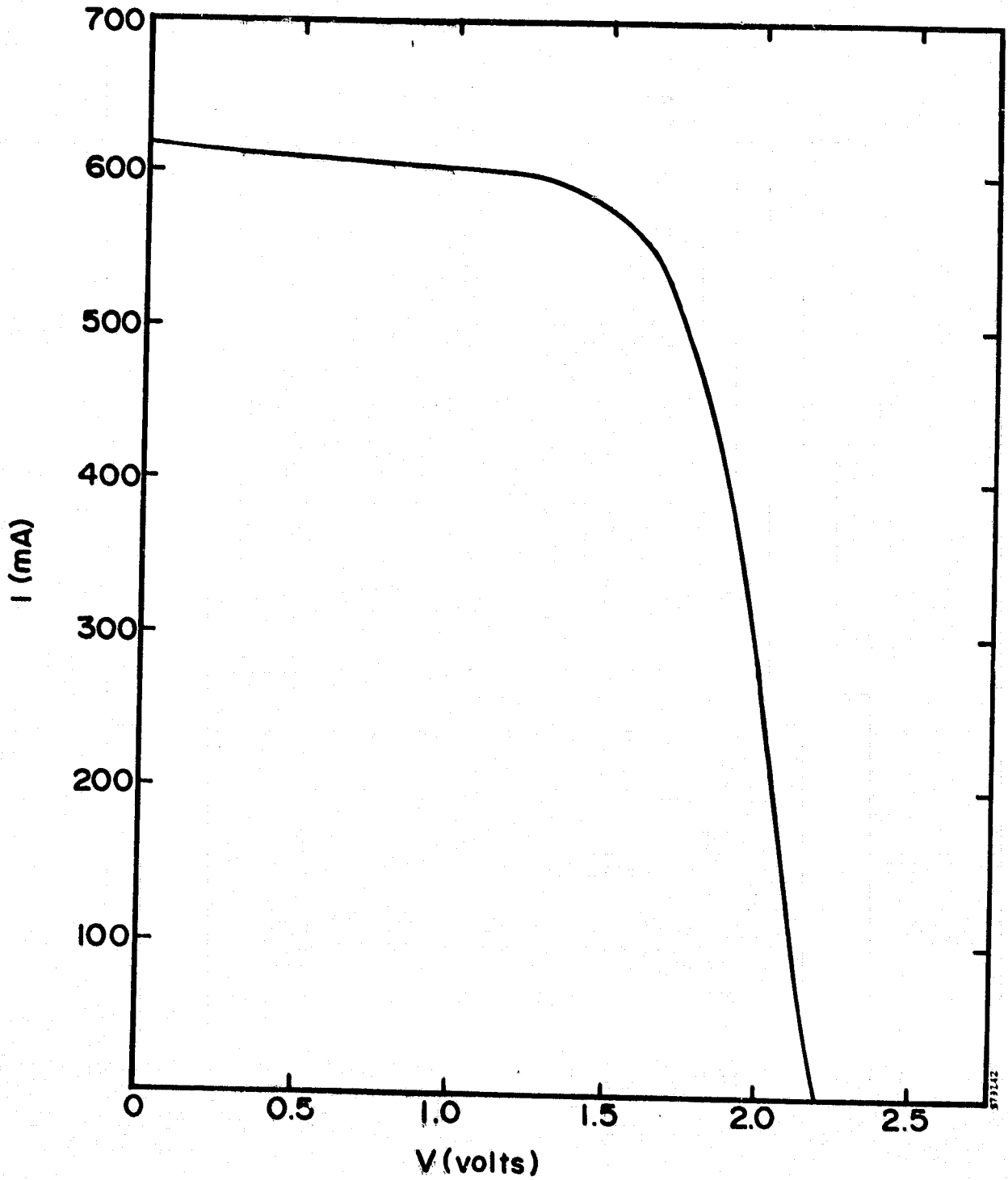


FIGURE 3-26. FOUR CELL MODULE WITH TOTAL GLASS ENCAPSULATION, TYPE II

A number of conventional backing systems for Type I modules have been demonstrated as replacements for those used during Phase I. While still not equal to an all-glass system in long term performance expectations, these backings represent a potentially practical and economically attractive alternative. Three conventional backings were demonstrated during Phase II: FVB/window glass, butyl rubber/Osnaberg cloth/aluminum foil, and EVA/aluminum foil. Four modules with each of the first two backings were prepared for the encapsulation review at the 9th LSA Project Integration Meeting, and underwent standard LSA module acceptance testing without any detectable mechanical or electrical changes. Seven modules received EVA/aluminum foil backs in preparation for the 11th LSA Project Integration Meeting. These have not yet undergone acceptance testing.

Substantial advances in Type II module development were also made during Phase II. A complete fabrication sequence for advanced, fully integral, all-glass encapsulated modules has been defined, and all of its components demonstrated. Completed modules have shown the feasibility of the process. The basic configuration of the advanced Type II module is shown in Figure 3-28, and a photograph and I-V curve of a complete module are presented in Figures 3-29 and 3-30.



**FIGURE 3-27. AM0 I-V CURVE OF FOUR CELL TOTAL GLASS ENCAPSULATED TYPE II MODULE**

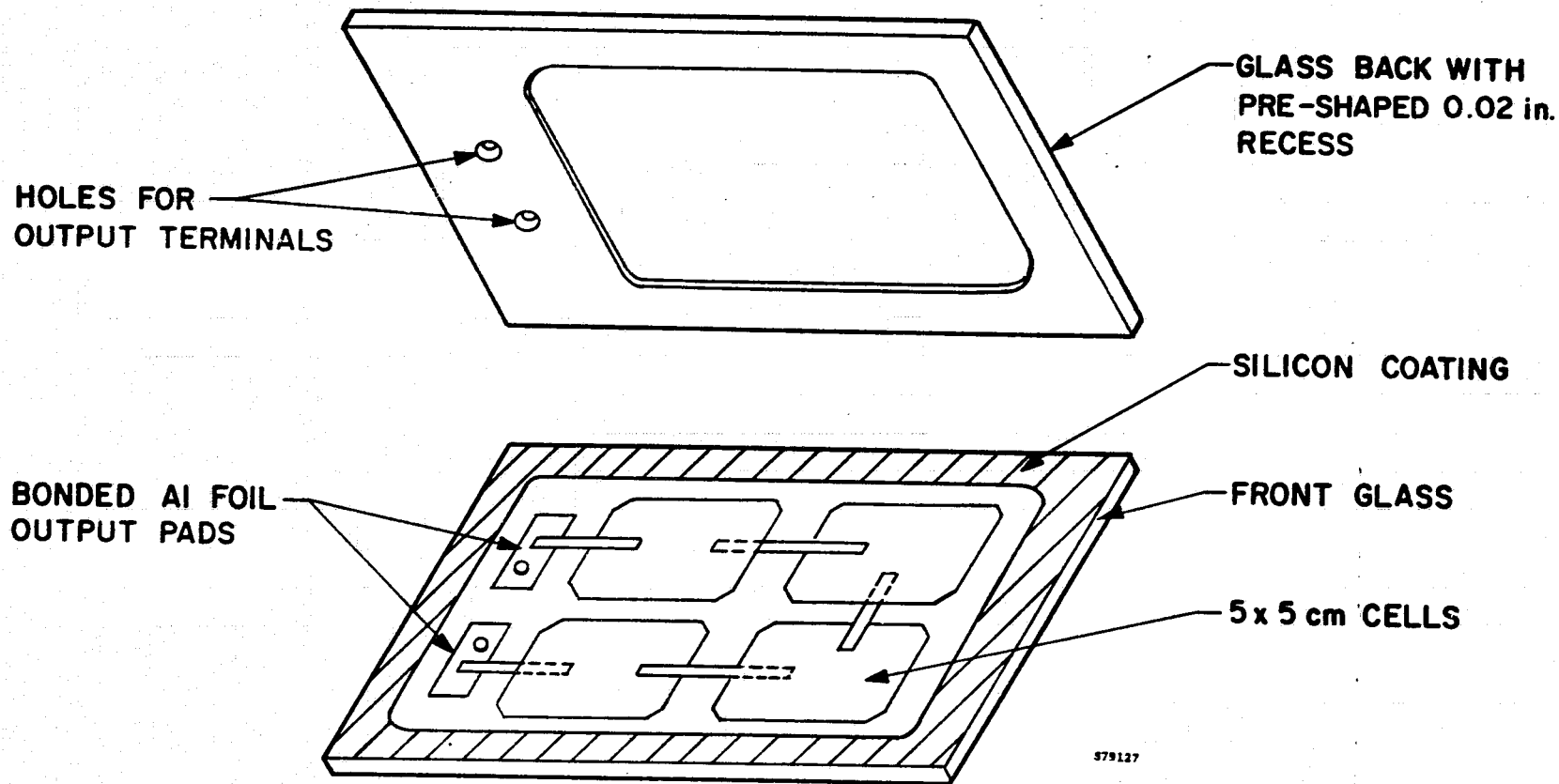


FIGURE 3-28. PRACTICAL ESB MODULE CONFIGURATION

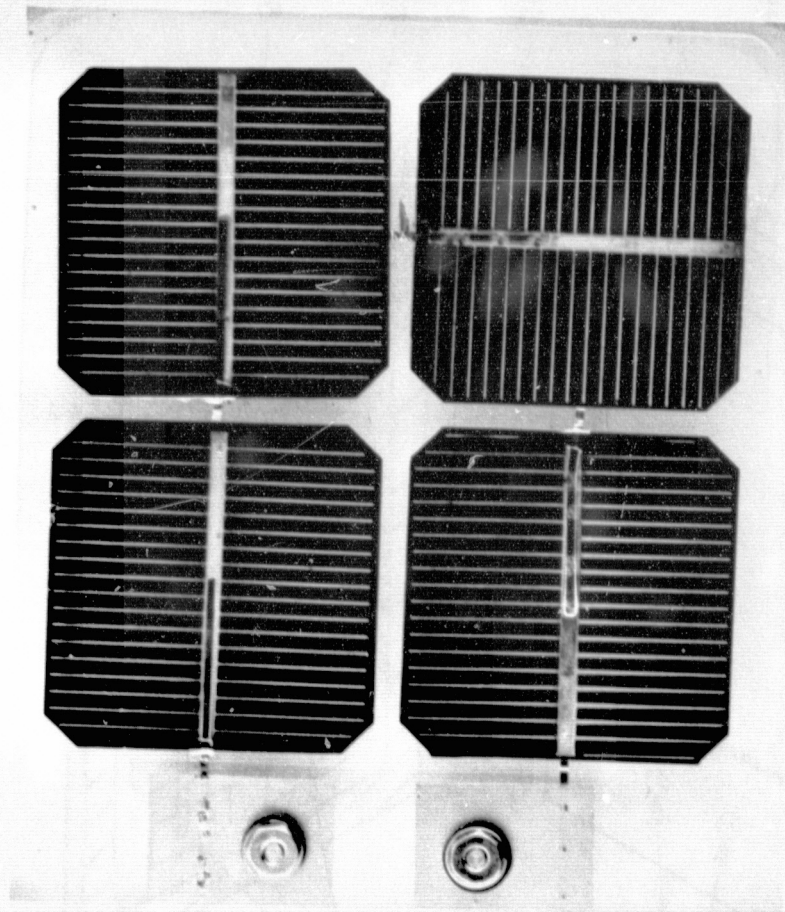


FIGURE 3-29. ADVANCED FOUR-CELL GLASS ENCAPSULATED  
MODULE

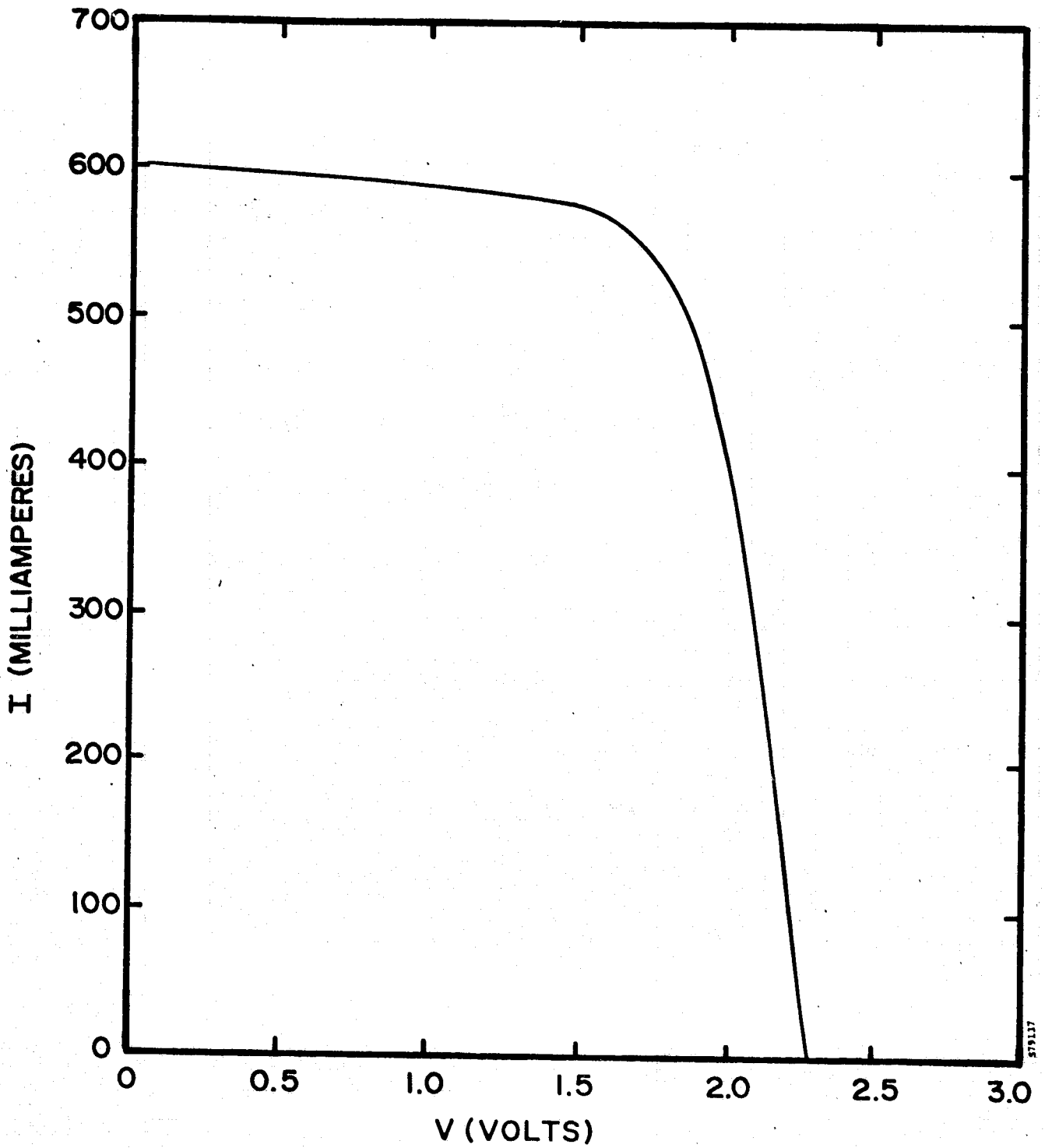


FIGURE 3-30. AM0 I-V CURVE OF ADVANCED FOUR-CELL GLASS ENCAPSULATED MODULE

Figure 3-31 outlines the fabrication sequence for a Type II module. Every step in this process has been thoroughly demonstrated at a developmental level, and there do not appear to be any fundamental obstacles to the evolution of the process into a routine, economical procedure. Considerable effort in the area of manufacturing engineering will, however, be required for large scale automated production.

The first process step is the application of a 1/2 inch wide dielectric layer to the perimeter of the front glass, to be used later as a glass-to-glass bonding medium. It is possible to reduce the width of the border considerably without jeopardizing the reliability of the module edge seal, permitting more efficient utilization of module area. For present, developmental purposes, a vacuum deposited layer of silicon is used. Although this material forms acceptable edge seals, a more economical method of application would be preferable. Separate tests have shown that inexpensive screen-printed, thick-film inks form strong, reliable bonds. Shear test results are reported in Section 3.7. In addition, two glass sheets, bonded together using Thick Film Systems' Silica Seal 1126, were immersed in boiling water continuously for 10 days, with no noticeable changes.

Metal foil pads are next electrostatically bonded to the front glass, to serve as the basis for future output terminals. The dielectric border is bonded to the glass at the same time. The hermeticity of the electrical output connections is a crucial element in module reliability. Moisture must be prevented from reaching the cell interconnections through the points of external electrical access. The output terminals used in Phase I all-glass modules consisted of aluminum pads bonded to a projection of the front glass, and connected to the cells by ribbons fed through the module edge seal, as shown in Figure 3-26. In Phase II, an improved terminal design, shown schematically in Figure 3-32, has been implemented. Holes drilled in the glass give access to the pads for the soldering of a brass terminal post, and provide mechanical support to the post. Bi-directional bonding of the pads to both front and back glasses forms a hermetic seal around the holes while providing a conducting path for electrical output.

Because it is easily bonded, 1-2 mil thick aluminum foil is now used for output pads, but it should be possible to use materials that are more compatible with conventional welding and soldering techniques. Tungsten, molybdenum, and Kovar foils have been investigated for this purpose, but no durable bonds have yet been formed. Thermal expansion mismatches may be responsible for the difficulties. A summary of these test results appears in Table 3-4.



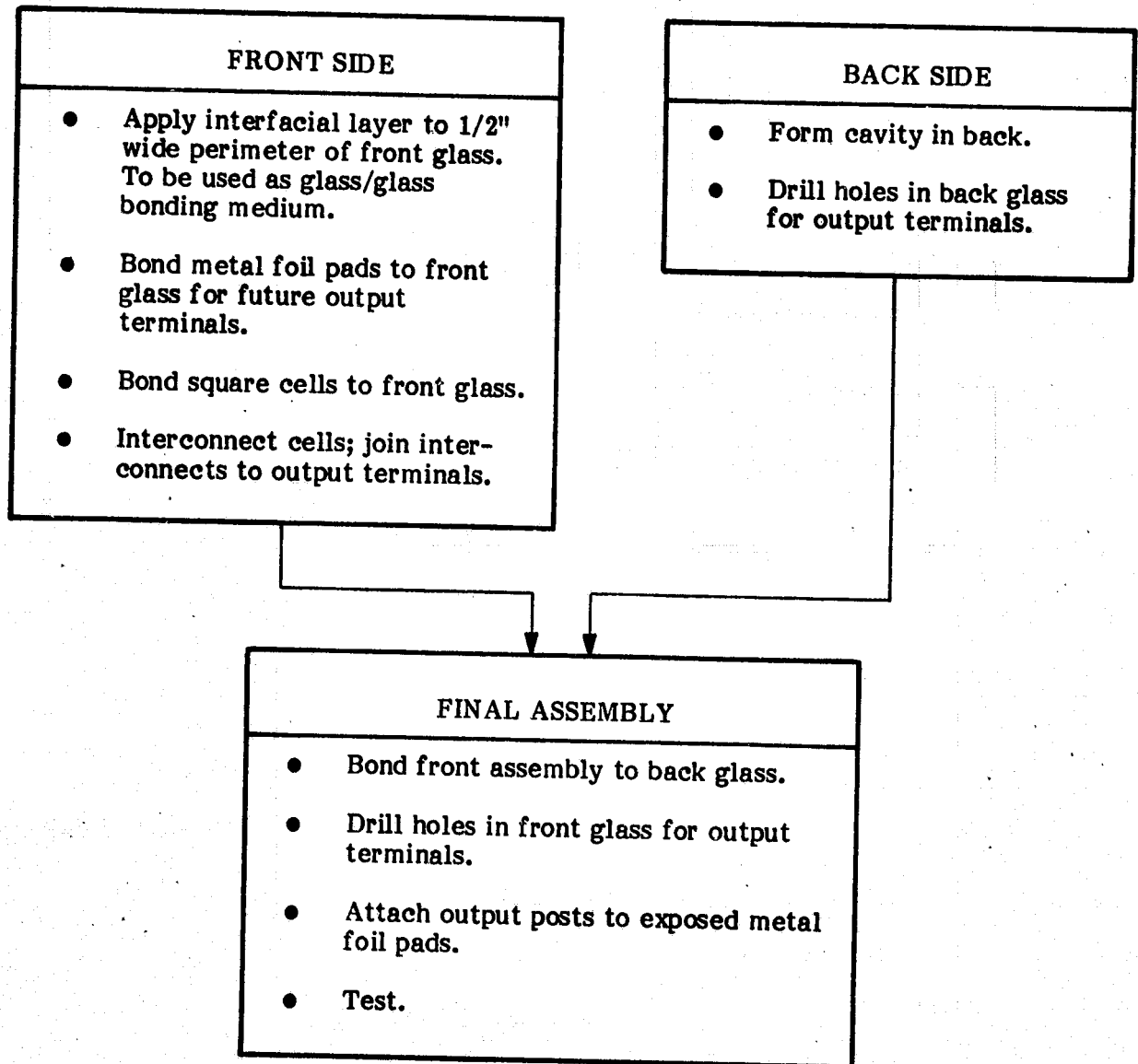


**FIGURE 3-31. FABRICATION SEQUENCE FOR ADVANCED TYPE II ALL GLASS ESB MODULES**

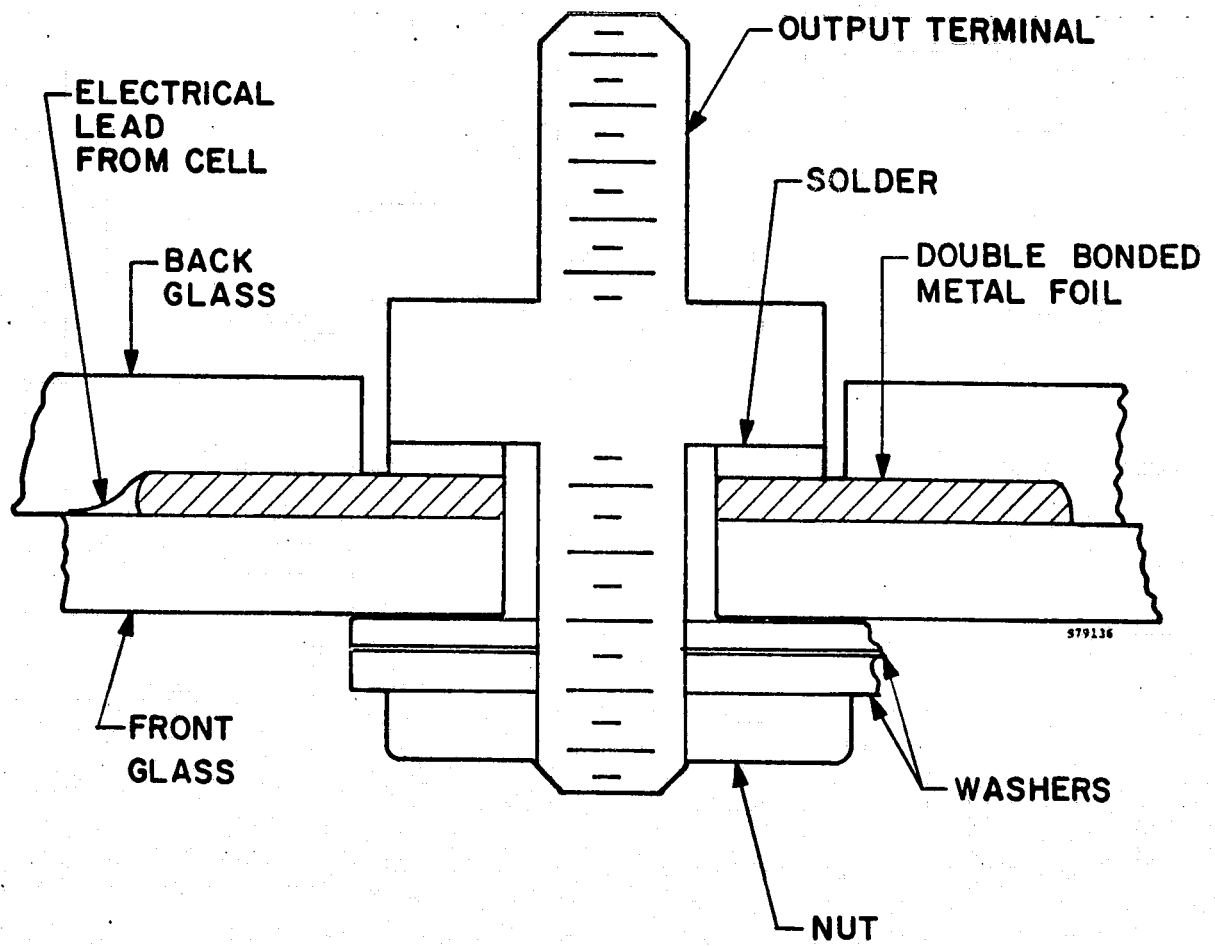


FIGURE 3-32. INTEGRAL MODULE OUTPUT TERMINAL DESIGN

TABLE 3-4. RESULTS OF ATTEMPTS TO BOND METAL FOILS TO 7070 GLASS

Temp.: Atm.:	580°C N <sub>2</sub>	580°C vacuum	600°C N <sub>2</sub>	600°C vacuum
Kovar	No bond	No bond	Temporary adhesion	No bond
Molybdenum	No bond	No bond	Temporary adhesion	No bond
Tungsten	Temporary adhesion	No bond	No bond	Splintered glass, indication of adhesion

It is in the next steps, the bonding of the cells to the glass and interconnecting them, that the most numerous, but also the most tractable, problems are encountered. Good bonding of the cells is not a major problem. Initial difficulties in obtaining uniform bonding at the center of the four-cell array proved to be due to nonflatness of the bonder plates, rather than to any fundamental problem with the bonding of tightly packed arrays. We have found proper bonding to be simply a matter of uniform pressure and correct choice of bond parameters.

The primary source of delays, failures, and inefficiencies in the present developmental process is the large amount of operator handling involved in preparing the modules for bonding, and in particular for preparing the ribbon interconnects for the bond cycle. Procedures and fixtures are already being implemented to simplify and systematize module setup. In a production line process, of course, operator handling of the unbonded module could and would be reduced to near zero.

A step in that direction is the use of a machined electrode, with cavities to hold the cells and interconnects in their proper positions. The electrode is to form part of a module alignment jig, shown schematically in Figure 3-33, which will permit simple, reliable, and reproducible alignment of cells and glass. Another potential process improvement is the replacement of silver ribbon interconnects with expanded silver mesh, which should simplify module assembly and improve interconnect reliability.

3-40

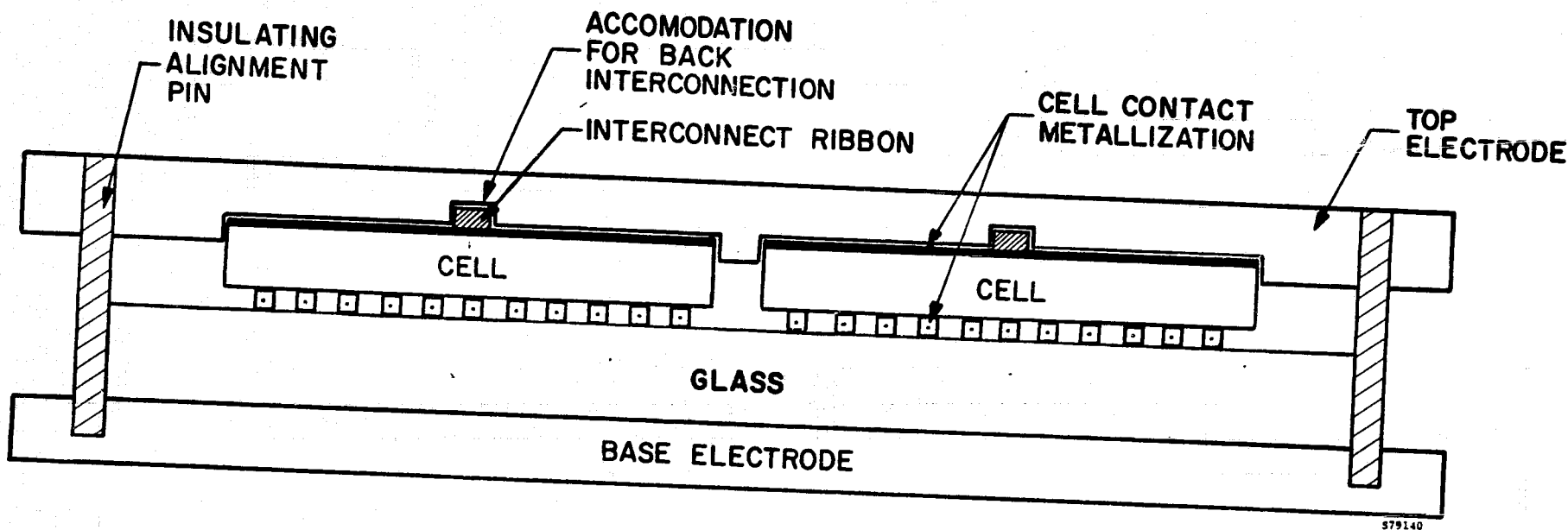


FIGURE 3-33. COMBINED ELECTRODE AND CELL ALIGNMENT FIXTURE FOR MODULE FRONT BOND

The encapsulation of the module is completed by the attachment of the back glass, which includes a cavity to accommodate the cells. Currently, these cavities are machined, which is not a cost-effective technique for large scale production. Representatives of Corning Glass Works, however, have indicated that hot pressing during glass fabrication is a practical, economical alternative. The back glass is electrostatically bonded to the dielectric border, forming a permanent, hermetic seal around the perimeter. At the same time, the bi-directional bond of the output pads is completed, hermetically sealing the output points. Although this process step is nearly routine, process optimization is required. Modules are now cooled on a table on which cooling takes place by conduction from below, but by radiation from above. The asymmetry results in warped module front glass assemblies. An annealing stage with symmetrical cooling should eliminate that problem and permit the use of a less harsh cycle for the back glass bond.

Advanced, Type II, all-glass-encapsulated modules have been delivered to JPL. The characteristics of two of these modules are listed in Table 3-5. Like their predecessors in Phase I, these are not intended to be practical, fully developed solar array modules. Rather they represent the integration of a large number of process steps, each of which has been independently shown to be adaptable to economical, large-scale production. As such, they demonstrate the feasibility of ESB as a practical solar module encapsulation system.

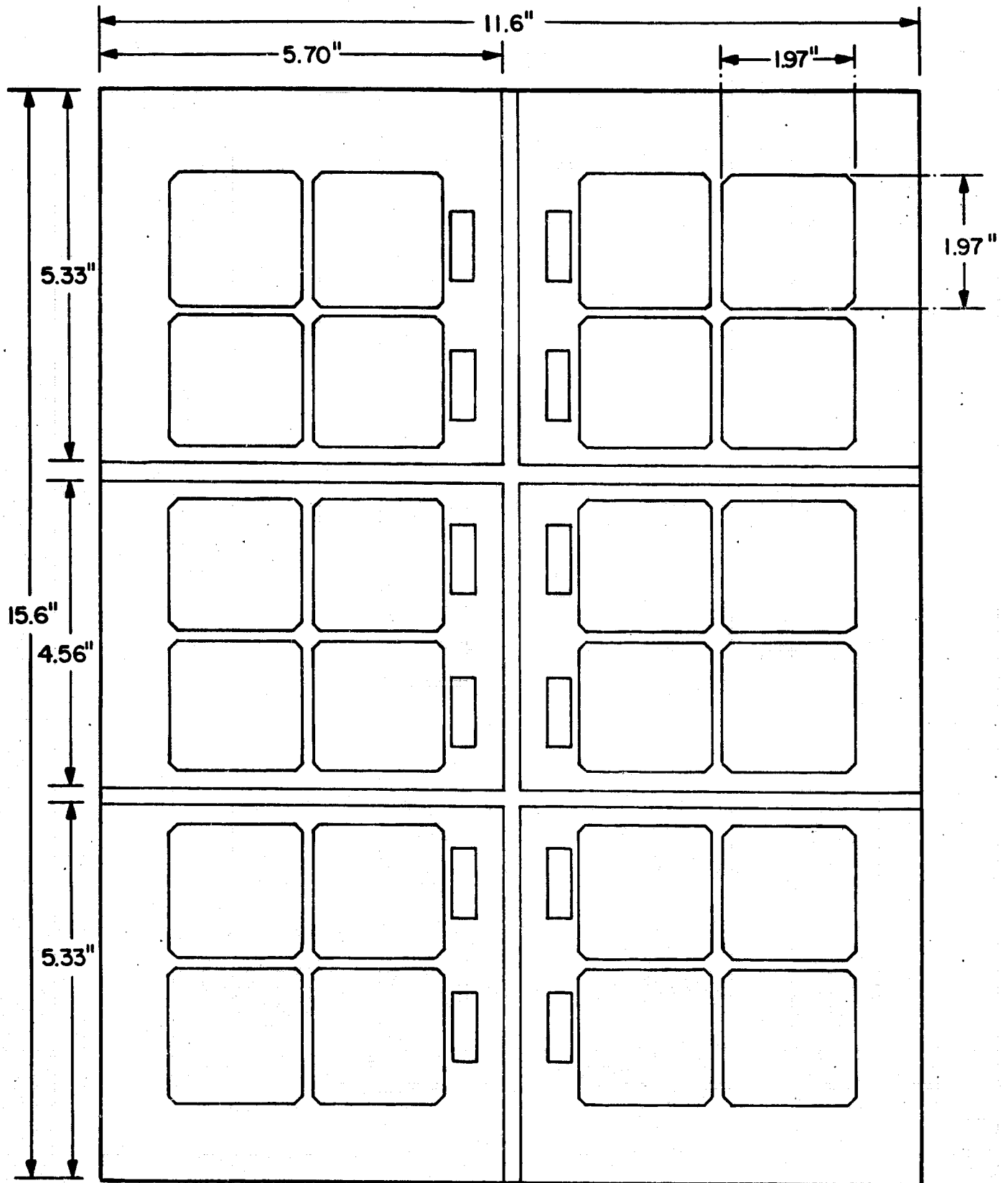
TABLE 3-5. SUMMARY OF ADVANCED TYPE II MODULES DELIVERED TO JPL

Module Number	M4002	M4003
Type	4-cell series	4-cell series
Metallization	Ti/Ag	Ti/Ag
Interconnects	Welded Ag ribbon	Welded Ag ribbon
Output Terminations	Screw posts	Screw posts
Antireflective Coating	Ta <sub>2</sub> O <sub>5</sub>	Ta <sub>2</sub> O <sub>5</sub>
V <sub>oc</sub> (volts)	2.16	2.15
I <sub>sc</sub> (mA)	720	734
P <sub>max</sub> (watt)	0.912	0.915
Curve factor (%)	58.6	58.0

The constraints of glass availability and present bonder size do not permit the production of single ESB assemblies as large as the JPL standard minimodule. Designs consistent with standard minimodule dimensions incorporate more than one multicell ESB assembly. The design used in Phase II uses six Type I assemblies, each containing four 5 cm square cells. These modules differ in no fundamental way from standard ESB front glass assemblies, and no anomalous problems have been encountered in their production. Seven ESB assemblies, sufficient for one minimodule, with one extra, were sent to JPL in preparation for the 11th LSA Project Integration Meeting. At JPL, the modules received a backing of EVA and aluminum foil. A support structure was also sent to JPL, to hold the assemblies firmly within the minimodule frame. The cell layout for this six-assembly design appears in Figure 3-34.

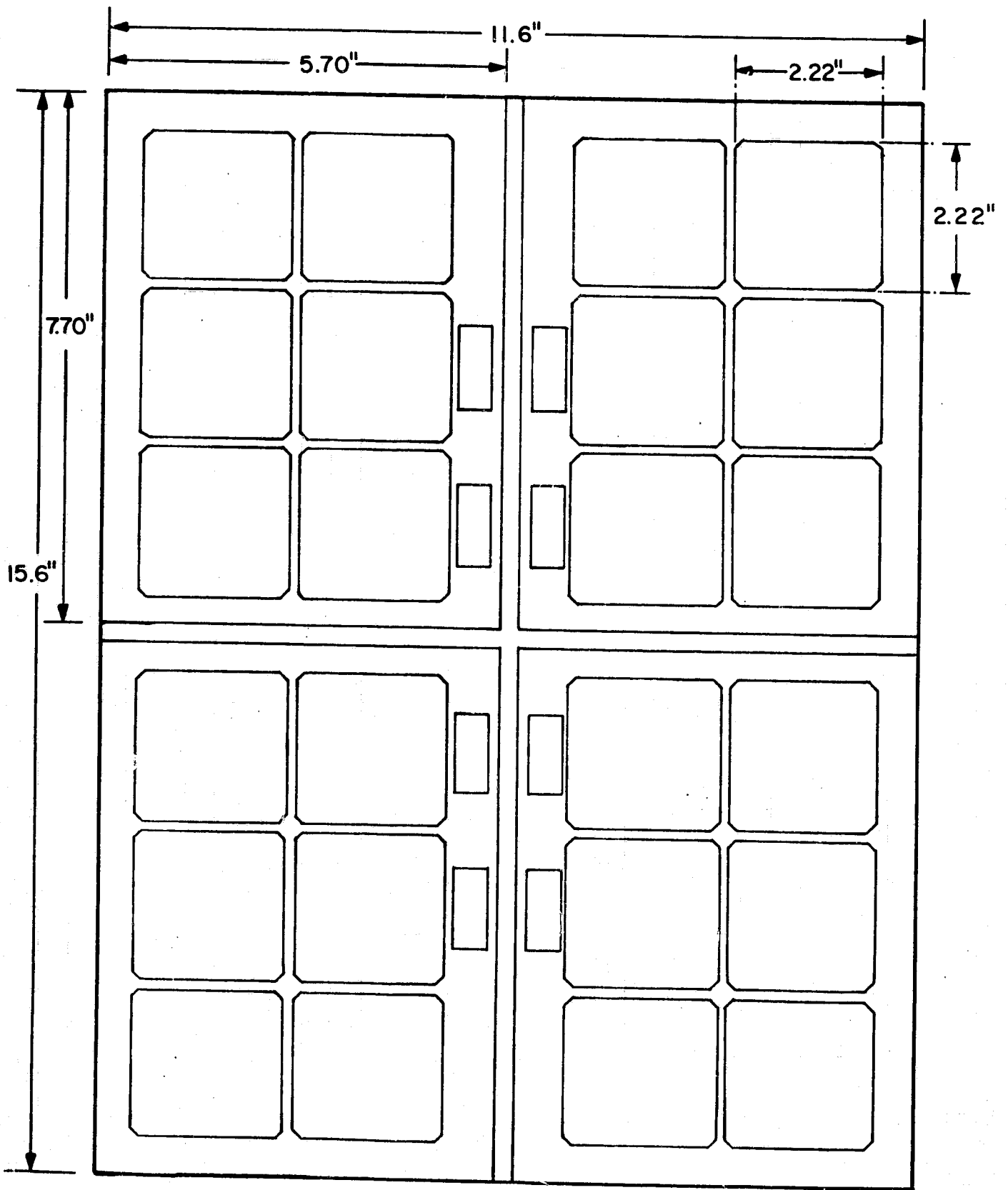
When larger sizes of Corning 7070 glass become available, and the tooling necessary for larger cells is obtained, early in Phase III, four ESB assemblies will be used, each incorporating six cells. The layout of this design is shown in Figure 3-35. These modules can be either Type I or Type II. The cells used will be approximately 5.6 cm square allowing increased use of the silicon wafer, and increasing the utilization of overall minimodule area from 56 percent to over 70 percent. The new cells will also use an improved metallization pattern, which should reduce power losses due to series resistance and shadowed area from the present 38 percent to below 17 percent. Fully independent contact points will permit the use of redundant interconnections, enhancing module reliability. Figure 3-36 is a drawing of the new cell design, showing the metallization pattern, and how the cell is cut from a 3 inch diameter wafer.

In all environmental tests performed to date, no electrostatically bonded module has shown any sign of electrical or mechanical degradation. Both all-glass encapsulated modules and integral front modules with a variety of backings have undergone standard LSA acceptance testing without any noticeable changes. Testing included thermal cycling — 50 cycles between  $-40^{\circ}\text{C}$  and  $+90^{\circ}\text{C}$ , at a maximum rate of  $100^{\circ}\text{C/hr}$  — and humidity tests, involving pre-dry and humidity soak cycles followed by 5 days at 90-95 percent relative humidity. Another Type I module with PVB/window glass backing has undergone one year of outdoor exposure at Bedford, Massachusetts, in an ongoing test, without any detectable physical or electrical degradation.



878003

**FIGURE 3-34. CELL LAYOUT FOR INCORPORATION OF SIX ELECTROSTATICALLY BONDED ASSEMBLIES INTO ONE MINIMODULE (APPROXIMATELY 1/2 SCALE)**



S78004

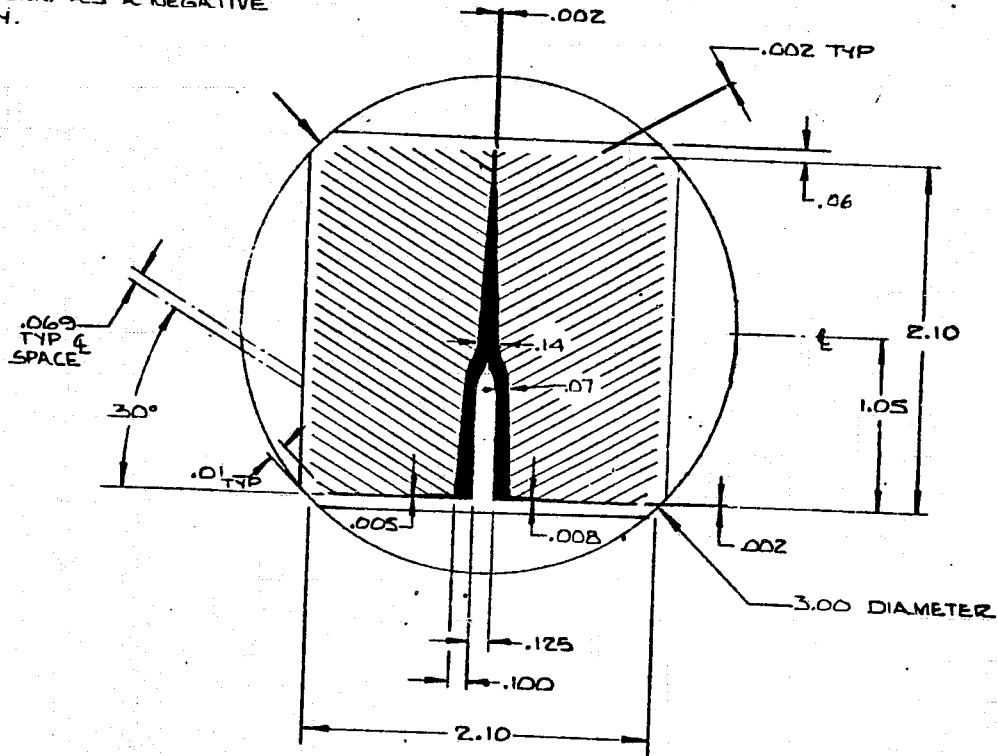
FIGURE 3-35. CELL LAYOUT FOR INCORPORATION OF FOUR ELECTROSTATICALLY BONDED ASSEMBLIES INTO ONE MINIMODULE (APPROXIMATELY 1/2 SCALE)



The information disclosed herein was originated by and is the property of Spire Corporation and except for rights expressly granted to the United States Government, reserves all patent, proprietary, design, use, sale, manufacturing and reproduction rights herein.

**NOTES**

1. THICKNESS & MATERIAL ARE NOT YET SPECIFIED.
2. PATTERN SHOWN AS A NEGATIVE FOR CLARITY.



REVISIONS				
ZONE/LTR	DESCRIPTION	DATE	APPROVED	
-	INITIAL RELEASE			

3-45

ITEM	ITEM	REQ	CODE IDENT. NO.	PART NO. OR IDENTIFYING NO.	DESCRIPTION	MATERIAL	SPEC
PARTS LIST							
DIMENSIONS ARE IN INCHES DIMENSIONS IN PARENTHESES ARE IN MILLIMETERS UNLESS OTHERWISE SPECIFIED TOLERANCES ARE				CONTR NO		NOV-30 1978	
DECIMALS				CONTR NO		SPIRE CORPORATION BEDFORD, MASS. 01730	
3 PLACE ± .002				DR. <i>E. Bon</i>		2/11/78	
2 PLACE ± .01				CHK. <i>...</i>		2/8/78	
1 PLACE ±				APPD			
FRACTIONS ±				APPD			
ANGULAR ± 1° 0'				CONTR DSGN ACT APPVL			
MATERIAL				FRONT ACT APPVL			
NEXT ASSY				USED ON		NOTE 1	
SIZE		CODE IDENT NO		DRAWING NO.		REV	
C		4D656		059-0107			
SCALE 2/1		SHEET 1 OF 1					

FIGURE 3-36. ADVANCED BONDER CELL DESIGN

### 3.7 BOND QUALITY EVALUATION

#### 3.7.1 Shear Strength Testing

A facility for testing the shear strength failure point of sample electrostatic bonds has been set up at Instron Corporation. Test samples consist of overlapping rectangles of glass with an overlap area of approximately 3 cm<sup>2</sup>. An evaporated coating of a film is applied to one side of the overlap, then electrostatically bonded to the other side.

Nine initial samples of dielectric films on both 7070 and 7740 glass were prepared to proof test the experimental facilities. These were pulled at 2 mm/min on the Instron Model 1122 test fixture. Results are shown in Table 3-6.

TABLE 3-6. PRELIMINARY LAP-SHEAR TEST RESULTS  
(All bonding done at 550°C)

Glass	Material	Bond No.	Bond Area (cm <sup>2</sup> )	Shear Force at Failure (kg)	Shear Strength (PSI)	Comments
7070	Nb <sub>2</sub> O <sub>5</sub>	46C-997	4.9	340	987	
7070	SiO <sub>x</sub>	46C-1003	4.0	118	419	clean shear
7070	Si	46C-987	4.5	216	683	clean shear
7070	Si	46C-989	4.0	211	750	
7740	Nb <sub>2</sub> O <sub>5</sub>	46C-714	2.5	110	626	
7740	Nb <sub>2</sub> O <sub>5</sub>	46C-871	2.5	120	683	glass failed, not interface
7740	SiO <sub>x</sub>	46C-870	2.4	95	563	
7740	Silica Seal 1126	46C-847	3.0	190	900	
7740	Silica Seal 1126	46C-850	3.3	520	2240	did not fail

Using these facilities, tests were made of the bond strength of various cell antireflective (AR) coatings applied to 7070 glass. The materials tested were:

Ta<sub>2</sub>O<sub>5</sub>  
 Nb<sub>2</sub>O<sub>5</sub>  
 CeO<sub>2</sub>  
 Al<sub>2</sub>O<sub>3</sub>  
 TiO<sub>2</sub>  
 ZrO<sub>2</sub>  
 SiO<sub>x</sub>  
 Si

Average results for these tests are listed in Table 3-7.

TABLE 3-7. AVERAGE SHEAR STRENGTH OF ANTIREFLECTIVE COATINGS  
 (All bonding done at 580°C)

Sample	Strength (PSI)	Standard Error*	N	Comments
Ta <sub>2</sub> O <sub>5</sub>	282	+ 45	4	all clean shear
Nb <sub>2</sub> O <sub>5</sub>	388	+ 153	6	mostly clean, glass cracked slightly
CeO <sub>2</sub>	204	+ 160	3	clean shear
Al <sub>2</sub> O <sub>3</sub>	412	+ 99	6	mostly clean shear some w/cracked glass
TiO <sub>2</sub>	750	+ 231	3	most broke glass
ZrO <sub>2</sub>	75	+ 44	4	most clean shear
SiO <sub>x</sub>	420	+ 154	5	most broke glass
Si	1107	+ 407	6	all broke or shattered glass

\* Error figure listed is one standard deviation of the mean. N is the number of samples tested.

Tantalum pentoxide ( $Ta_2O_5$ ) normally has been used for bonded cells. It is seen that although  $Ta_2O_5$  does not form the strongest bonds of any AR coating tested, it does form the most consistent, and thus may be the best choice.  $TiO_2$  had the strongest measured bond strength of the AR coatings tested (Si is not an AR coating, and was tested to provide a control sample), so  $TiO_2$  may be a better choice than  $Ta_2O_5$ , although  $TiO_2$  bond strengths were less consistent.  $CeO_2$  was previously reported as not forming electrostatic bonds. It is seen here that under controlled bonding conditions, it is possible to form bonds with  $CeO_2$ , although the bond strengths vary greatly.

The strength figure for the control coating, pure silicon film, compares well with that reported previously<sup>(6)</sup> from shear tests done at JPL, 1390 PSI. The difference is within one standard error of the mean. It should be noted that the previous tests were done with type 7740 glass.

Four samples were mistakenly bonded at 750V rather than 1000V bond potential: two  $Al_2O_3$ , one  $ZrO_2$ , and one Si. These were not included in the averages listed. It is interesting to note that in three out of these four cases, the low voltage bond was the lowest or near lowest measured strength, showing a possible correlation between bond strength and bond parameters. This was investigated further during the bond parameter test matrix studies discussed in the following section.

### 3.7.2 Electrostatic Bonding Process Studies

Using the standard lap-shear test configuration, the bond strengths of silicon films were investigated as a function of bond current, voltage, and charge transfer. Both constant current and constant voltage bonds were investigated. Table 3-8 shows the test conditions. Five samples were tested at each bond cycle, 105 samples total. The microprocessor performed an integration of the total current running through the sample, and shut off power when the total specified charge transfer was reached. If this charge transfer did not occur within a set bond time (9 1/2 minutes in most cases, but up to 25 minutes in cases of very large charge transfer at low currents), the bond was terminated at that time.

All bonds were done with set absolute limits of 1500V and 25 mA. Thus, if a constant current bond required higher voltage than this maximum, the voltage would stop rising at this limit. Likewise, current was limited to 25 mA during constant voltage bonds.

**TABLE 3-8. ELECTROSTATIC BONDING PARAMETER TEST SCHEDULE**  
 (All bonds made at 575°C)

(Note: Configurations tested are marked with X's.)

**1. Effect of Bond Current and Total Charge Transfer on Bond Strength - Constant Current Bonds**

Total Charge Transfer (Millicoulombs)					
Bond Current	90	180	360	720	1440
6.0 mA	X	X	X	X	X
3.0 mA	X	X	X	X	X
1.5 mA	X	X	X	X	X

**2. Effect of Bond Voltage and Total Charge Transfer on Bond Strength - Constant Voltage Bonds**

Total Charge Transfer (millicoulombs)					
Bond Current	90	180	360	720	1440
1.0 kV	-	-	X	X	X
0.5 kV	-	-	X	X	X

To eliminate machine dependent effects, processing order was constructed such that, in general, no two bonds of the same parameter set were bonded in the machine in the same five sample cassette. The maximum stress recorded in this test was 4789 PSI, for a sample bonded at 1.5 mA with 0.72 coulomb total charge. Average stress was 1650 PSI  $\pm$  130 PSI, notably higher than the value of 1107 recorded during the AR coating test. Whether this is due to statistical variation, the changes in bond parameters, or increased skill at the test equipment is unknown. Samples with shear strength over 2000 PSI were prone to glass failure, so in many cases values found were only a lower limit to the actual bond strength.

Figures 3-37, 3-38, and 3-39 display some results of this matrix study. Error bars shown on these figures are one standard deviation of the mean value. Figure 3-37 shows that there was no significant difference in bond strength for samples bonded at various constant current levels. In the next two graphs, all current levels were averaged. Figure 3-38 shows the results of different voltages. The 1500V point in this figure is the average of all the constant current bonds, run at a voltage limit of 1500V. This shows that for bond voltages under 1000V, there is a dramatic drop in bond strength. Figure 3-39 shows bond strength plotted against charge transfer setting. Up to a point, the bond strength increases with charge setting. The cause of the possible drop at very high charge transfer is unknown.

These data suggest:

1. There is a voltage threshold below which bonding will occur poorly or not at all.
2. Bond strength is essentially independent of the value of current flow through the sample.
3. Bond strength is weakly correlated to the charge transfer level.

It should be noted that these results may be a function of bond temperature.

### 3.7.3 Empirical Study of Module Bonds

In addition to the experiments conducted on bond strength, an attempt has been made to find an empirical relationship between bond parameters — particularly charge transfer — and the bond area coverage observed in module bonds. The numerous process variations and other variables affecting module bonds leave such a study a long way from an entirely systematic experiment, but it can nevertheless yield some information.

Figure 3-40 depicts the current and voltage as a function of time for a typical module front bond, as logged by the Tektronix 4051 microprocessor. The current is thought to consist of two components: an exponentially decaying ionic flow, which forms the polarized region in the glass that allows bonding to occur, and a steady-state electronic current that is not involved in the bonding process. Since the charge transfer listed on the graph is obtained by simple integration of the total current, it is affected

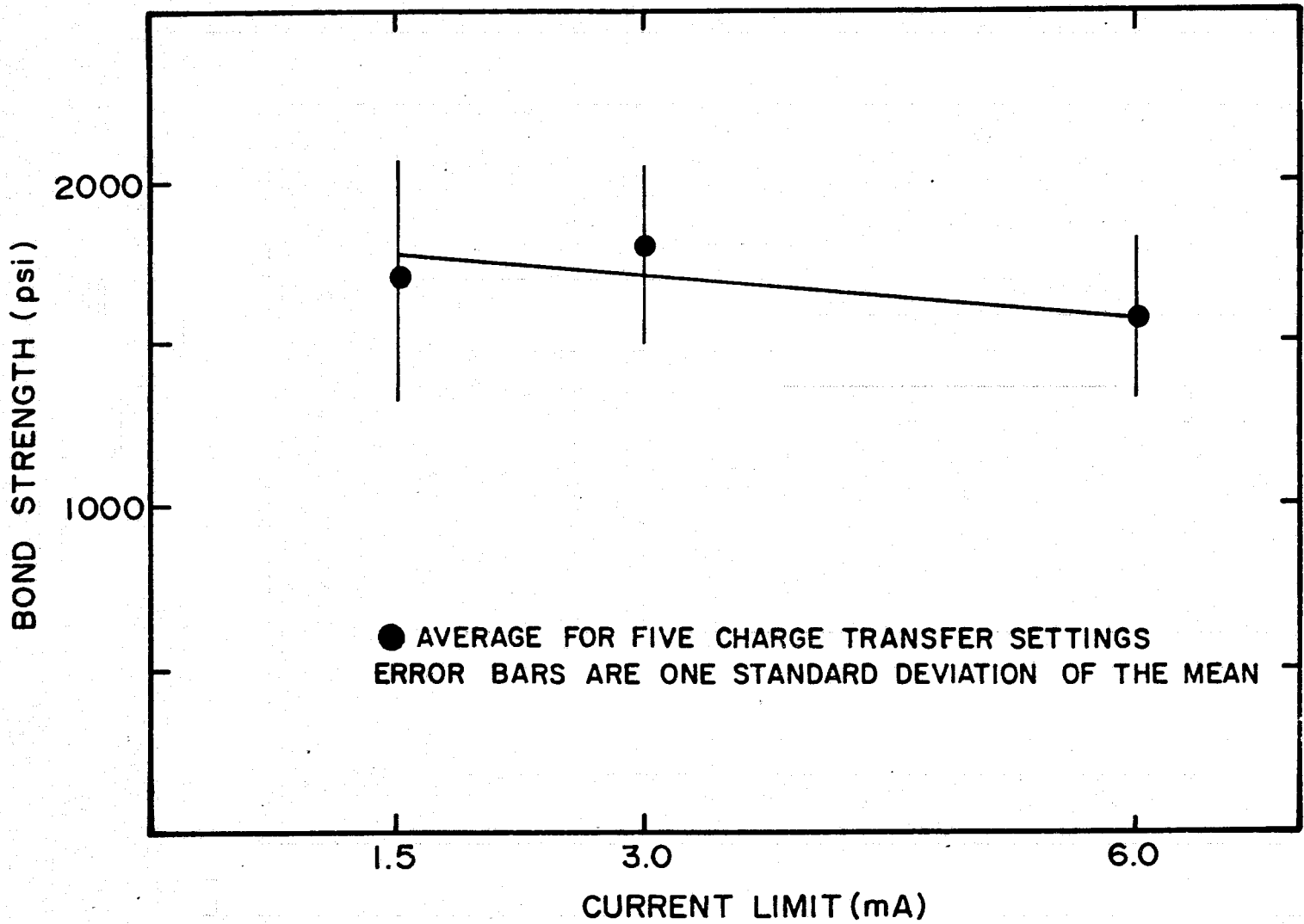


FIGURE 3-37. BOND STRENGTH VERSUS CURRENT LIMIT SET

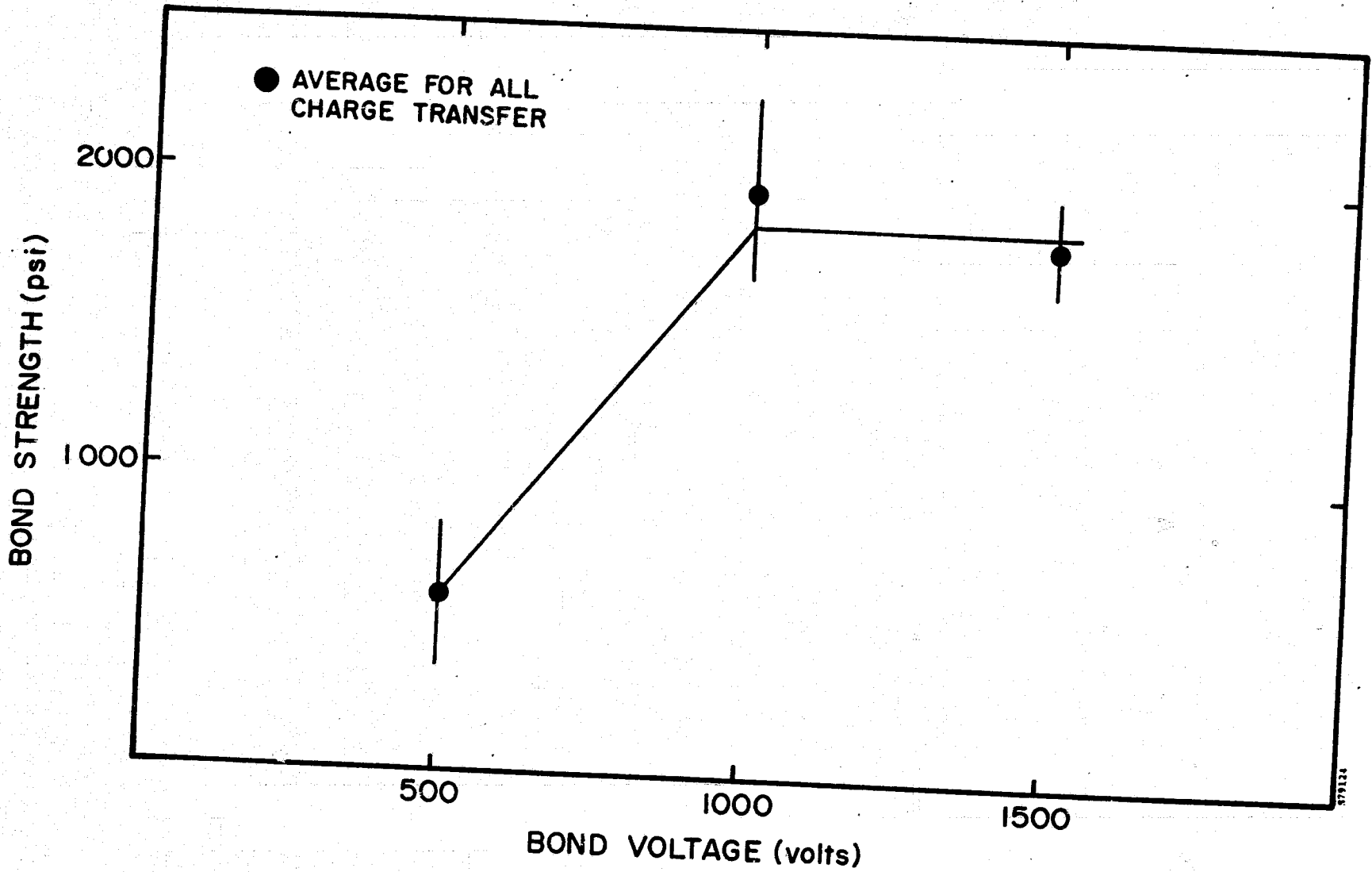


FIGURE 3-38. BOND STRENGTH VERSUS BOND VOLTAGE



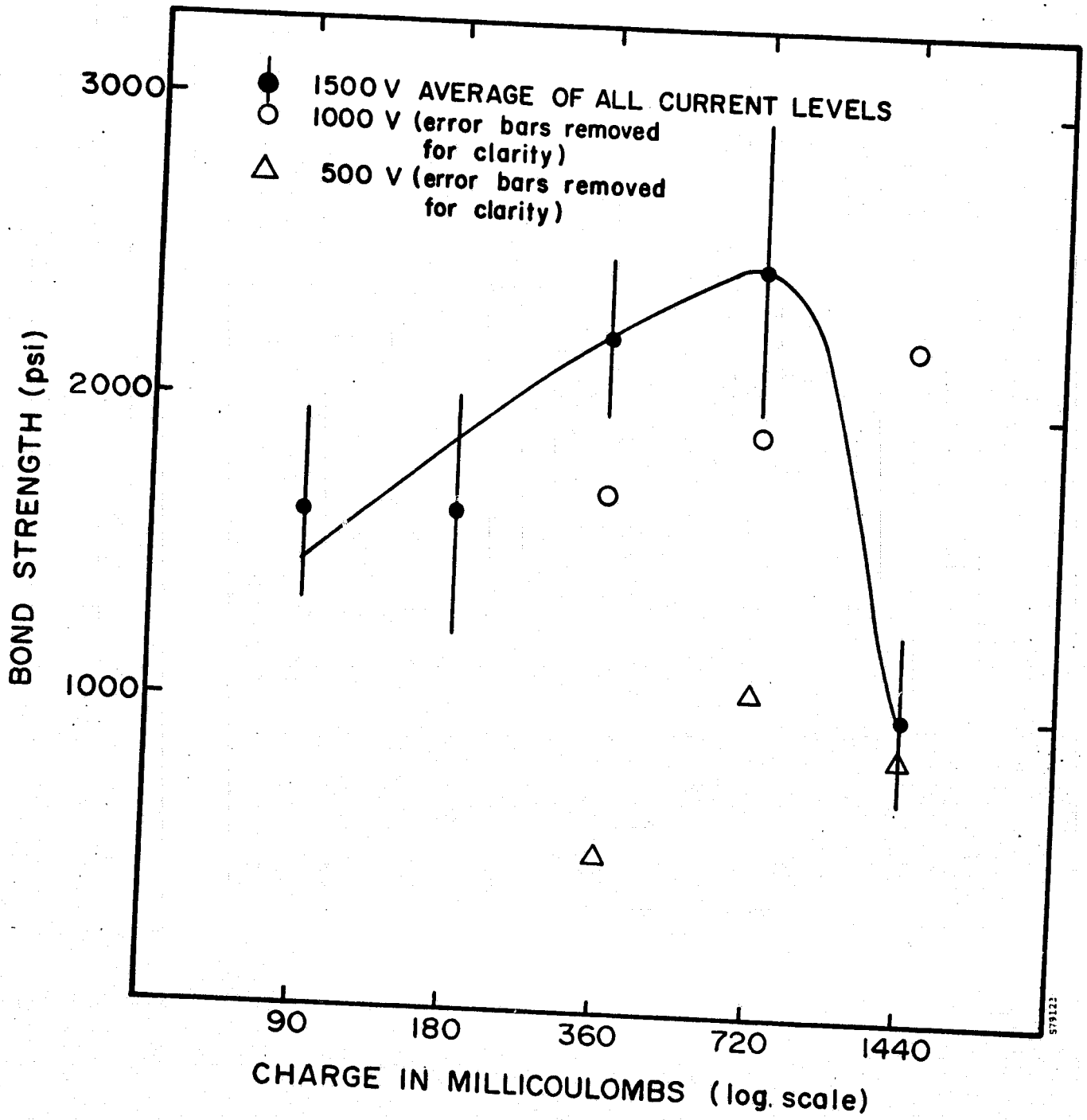


FIGURE 3-39. BOND STRENGTH VERSUS CHARGE TRANSFER SETTING

Bond 46c-1955

DATE: 39

TIME: 13:46

Max bond current = 103.27 Maximum voltage = 917.4 Charge transfer = 9.36

3-54

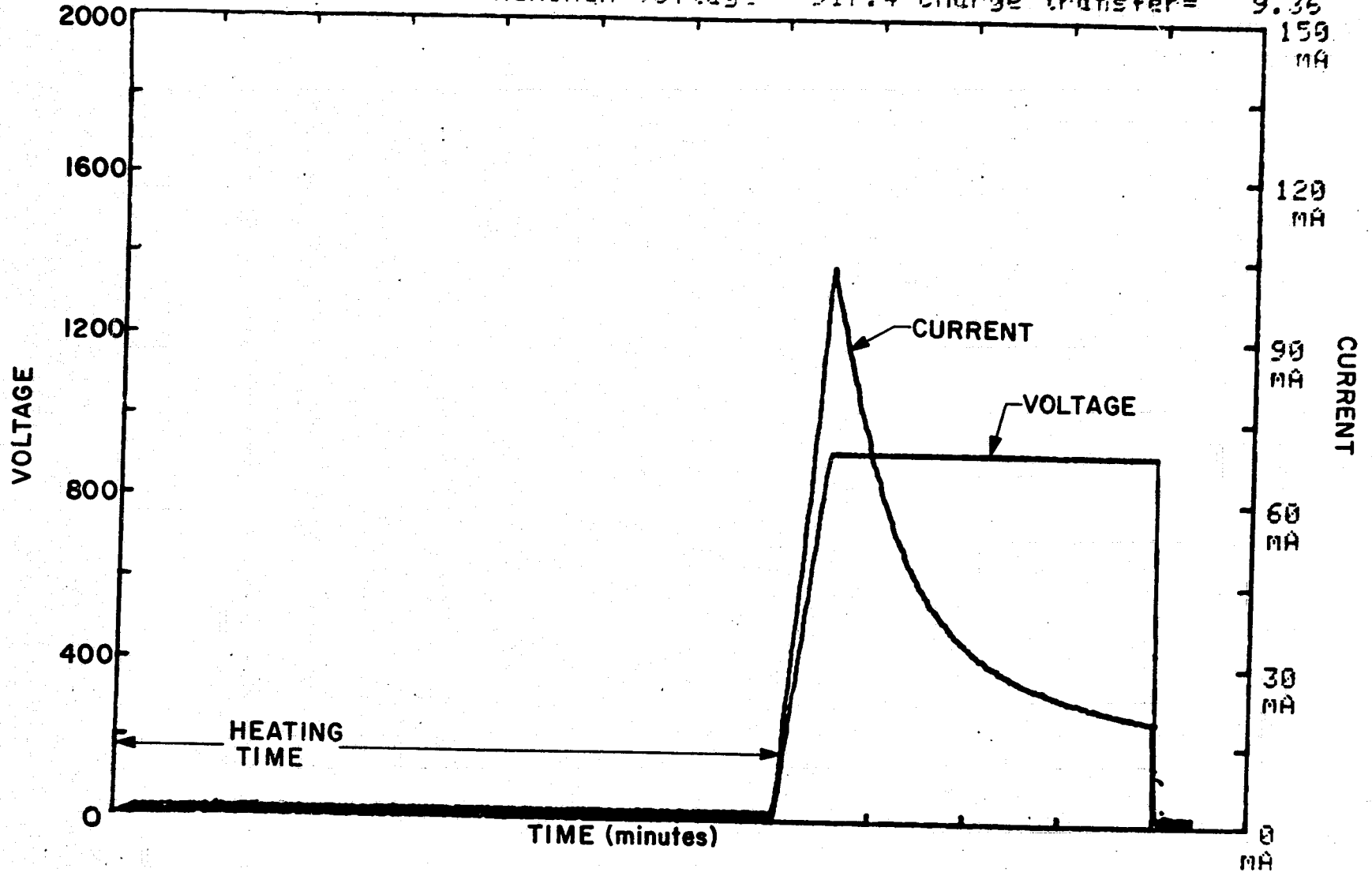


FIGURE 3-40. CURRENT AND VOLTAGE CHARACTERISTICS OF A MODULE FRONT ASSEMBLY BOND

very strongly by the electronic component, which can vary substantially from sample to sample. As a result, an attempt to find a connection between total charge transfer and bond coverage yielded a correlation coefficient of  $-0.01$  — indicating no relationship at all.

A much stronger correlation was found when bond area was related to a quantity designated "net charge" and intended to approximate the ionic component of the integrated current. It was calculated by subtracting from the total charge transfer a term due to the electronic current, assumed constant and equal to the current at the end of the bond. Such calculations could not be made for the bonds reported in the last section, due to the extremely low currents involved. When the relationship between this variable and bond coverage was investigated, a correlation coefficient of  $0.56$  was found, for a sample of 16 module bonds. Figure 3-41 shows the least squares fit to the data. Although the correlation is not strong, it is sufficient, considering the number of variables left uncontrolled, to suggest the existence of a real relationship between ionic charge transfer and bond coverage.

### 3.8 INVESTIGATION OF THE PHYSICS OF ELECTROSTATIC BONDING

Several surface analysis techniques have been considered for investigating bonding physics. Initial analyses used tantalum films electrostatically bonded to glass. These were studied by Auger electron spectroscopy and by helium ion backscattering. The helium ion backscattering detected no difference between bonded and unbonded tantalum films.

Two separate Auger studies were conducted on the bonded and unbonded tantalum films. Oxygen concentration in the tantalum was seen to rise as much as 60 percent near the glass interface in the bonded film. Figures 3-42 and 3-43 show results of one of these studies.

Further Auger studies were done with aluminum films. Aluminum was selected because it forms strong electrostatic bonds, it evaporates well, and it has Auger peaks well separated from those of oxygen, silicon, and boron. Charging of the glass by the ion sputtering beam turned out to be a major problem. This problem was worst for the 1000A and 1500A films, and prevented the gathering of useful information from the glass side of the interface. The optimum film thickness for this analysis was 2000-3000A. No significant differences between bonded and unbonded samples were found.

3-56

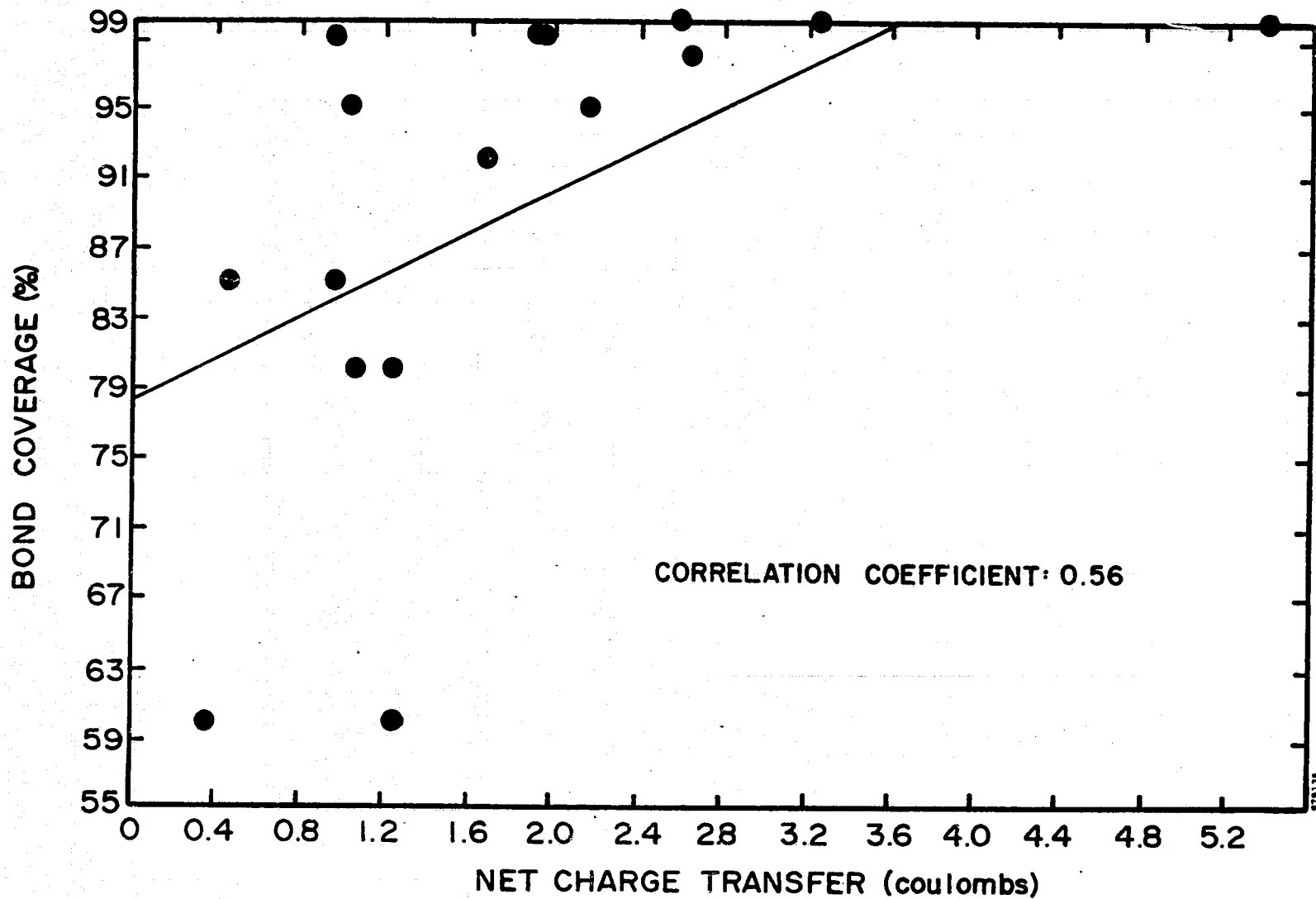


FIGURE 3-41. BOND COVERAGE VERSUS NET CHARGE TRANSFER FOR MODULE FRONT BONDS

3-57

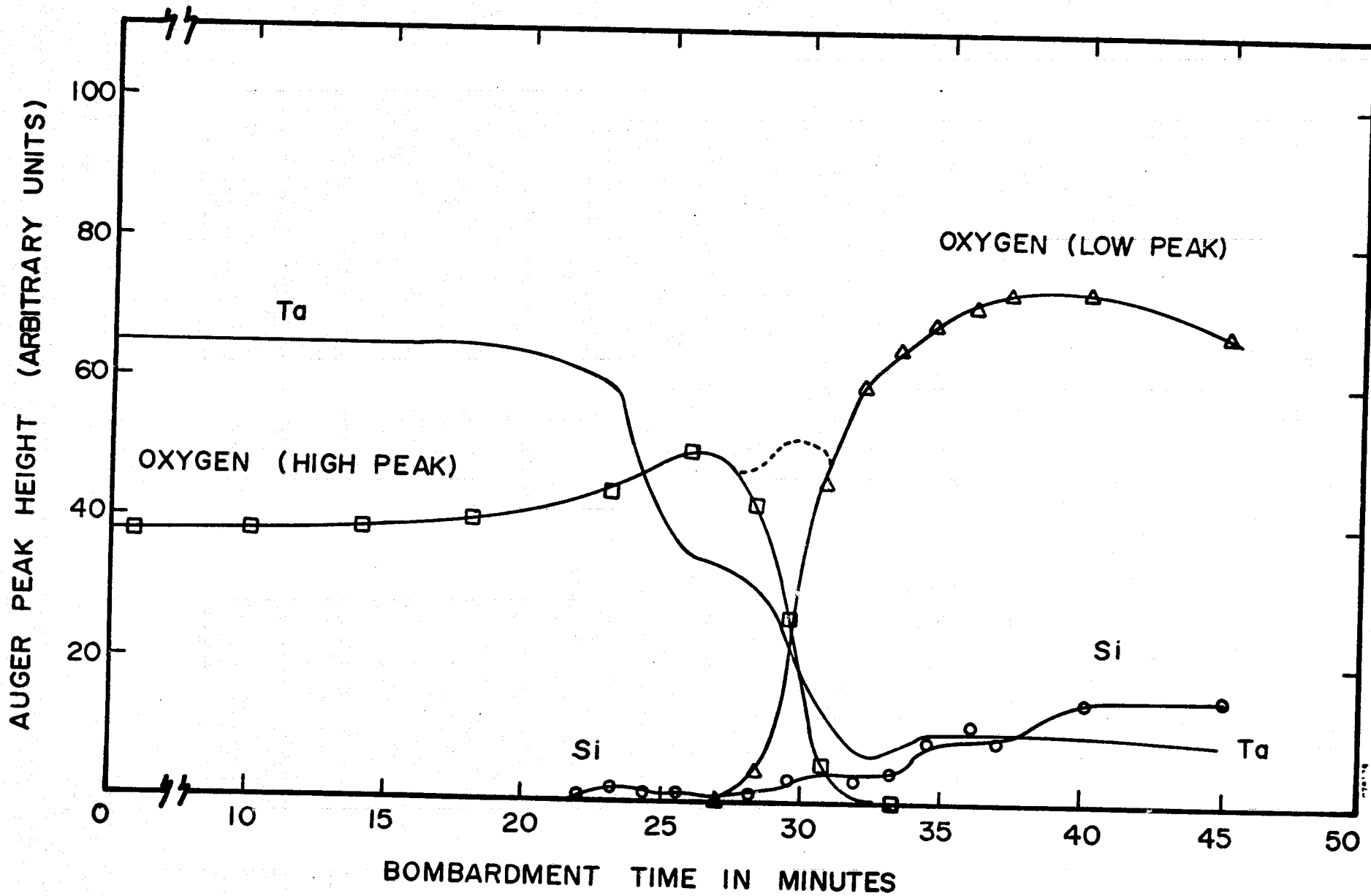


FIGURE 3-42. AUGER DEPTH PROFILE OF UNBONDED TANTALUM FILM ON 7070 GLASS

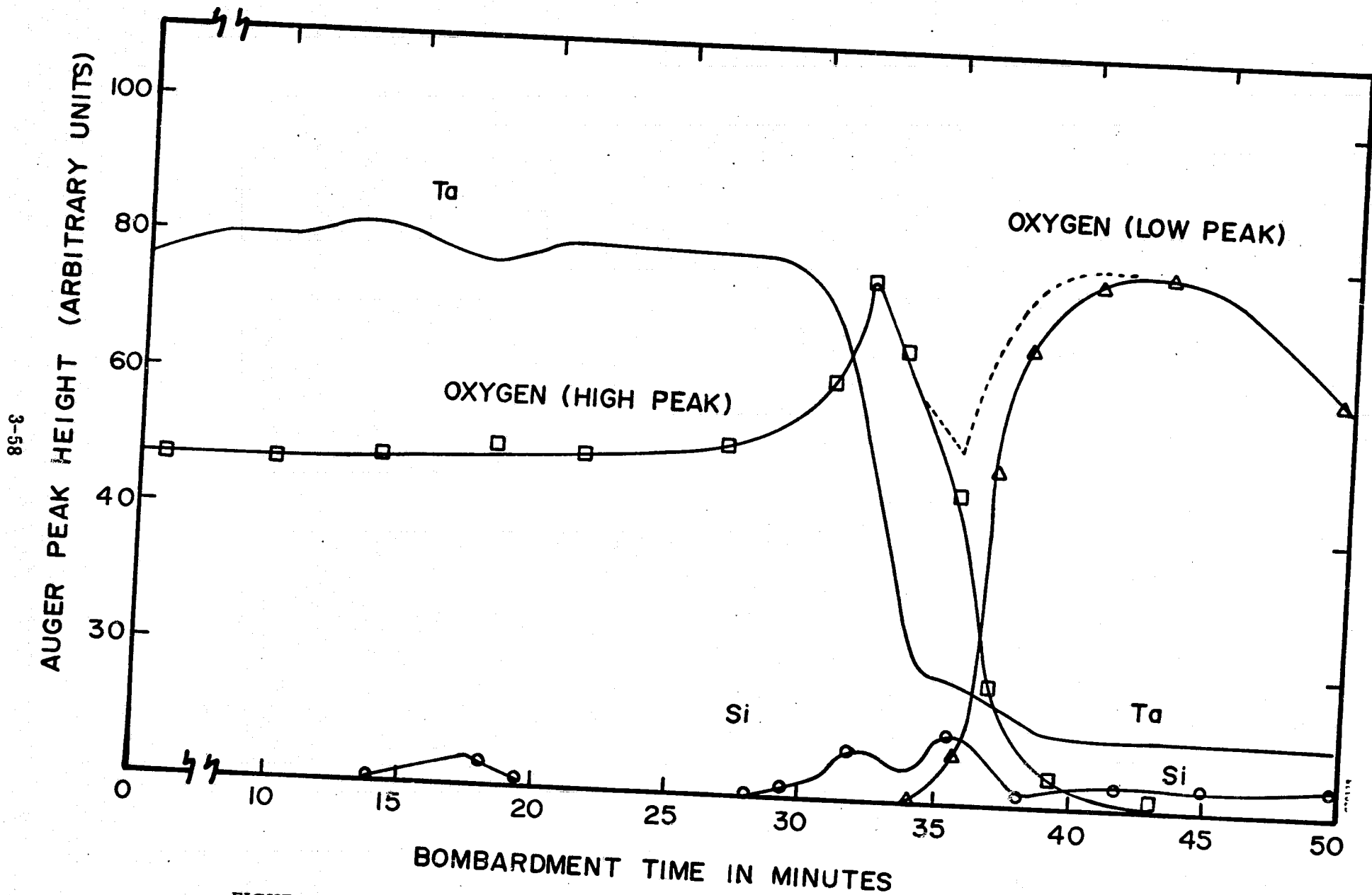


FIGURE 3-43. AUGER DEPTH PROFILE OF ELECTROSTATICALLY BONDED TANTALUM FILM ON 7070 GLASS

### 3.9 ECONOMICS OF INTEGRAL GLASS ENCAPSULATION

Electrostatic bonding offers significant potential for low cost solar array encapsulation. This potential comes from the simplicity of the process which requires few consumable materials to form the module and from the applicability to automated in-line processing.

The ultimate cost of ESB encapsulation will be driven by the cost of the borosilicate glass used. Present cost of 7070 glass from Corning Glass Works is high because of the very low demand for this particular product. Three manufacturers of borosilicate glass have been consulted regarding ultimate cost of this material. All have responded that the high cost of borosilicate glass is due mainly to the low demand. While raw materials cost and energy consumption during fabrication are somewhat higher than for soda lime glass, it is production volume that controls the price.

One manufacturer, Corning Glass Works, has presented a development plan for producing sheet borosilicate glass in high volume. This plan, shown in Table 3-9, would result in a glass price of \$0.45/sq ft based on a one time production volume of 50 million square feet. A price of \$0.30/sq ft was projected for a production volume of 150-200 million square feet. These volumes are still very low on the scale of ultimate solar array requirements or present-day soda lime glass production. Thus, it can be seen that borosilicate glass prices will be low enough for electrostatic bonding to be a cost-effective process for solar array encapsulation.

Based on these prices estimates of array fabrication cost have been prepared for the two fundamental module designs developed under this program. These are the all glass, full ESB module and the ESB front, conventional back module. The encapsulation cost projections are given in Table 3-10.

The cost for the system with ESB front and conventional back is near the LSA Project 1986 goal of  $\$0.027/W_{pk}^{(7)}$  for encapsulation materials. The all-ESB system is above the materials cost allocation by  $\$0.024/W_{pk}$ . However, since encapsulation by electrostatic bonding is a part of assembly, the total cost of both materials and processing must be examined. Electrostatic bonding is a process that lends itself to automation easily. Therefore, total system costs for both module designs will probably be within 1986 guidelines. During Phase III of this program, requirements for process scaleup to practical size will be examined. This study should provide sufficient detail for a SAMICS analysis of the total encapsulation cost.

TABLE 3-9. CORNING GLASS WORKS SHEET GLASS DEVELOPMENT PLAN

Key Tasks	Timing	Responsibility	CGW Product	Projected Volume/ Target Price (\$/ft <sup>2</sup> )
1. Forming Compatibility & Composition	Ongoing	CGW	Drawn & Rolled Sheet Compatibility	Ongoing
2. Process Refinement and Testing of New Candidates	3rd Qtr. 1978	Spire	6 1/2" Squares 7070	250-499 Pieces 4MM \$7.95/Piece
3. 7070 Size Increase	As Required	JPL	8" Squares Hand Pressed 7070	250-499 - \$19.65 Each
4. Hand Rolled Large Sheet 7070	As Required	CGW	7070 1' x 4'	\$1000/Run 2-3 Pcs/Run Maximum 10 Pieces
5. Large Electrostatic Bonder Justification	3rd Qtr. 1978	JPL/Spire	—	—
6. Large Electrostatic Bonder Ordered	1st Qtr. 1979	JPL/Spire	—	—
7. JPL Commit Funding 7070 Melt Danville, VA	1st Qtr. 1979	JPL	Approximately 1' x 4' x 0.1' 7070	A. 400 Sheets \$75M B. 4000 Sheets \$160M C. 8000 Sheets \$270M D. 16000 Sheets \$430M
8. CGW 7070 Melt Danville, VA	3rd Qtr. 1979	CGW	Approximately 1' x 4' x 0.1' 7070	A. \$46.88/Sq. Ft. B. \$10.00/Sq. Ft. C. \$8.44/Sq. Ft. D. \$6.72/Sq. Ft.
9. Production Scale Up Based on JPL Volume	1980-1982	CGW	Approximately 1' x 4' x 0.1' 7070	By 1982 \$1.50/Sq. Ft. @ 1 Million Sq. Ft.
10. Increase Process Capacity to Meet 1985 Goals	1982	GCW/JPL/ Spire	To Be Determined	\$0.45/Sq. Ft. @ 50 Million Sq. Ft.

Note: 1982 and 1985 price projections are based on 1975 dollars.



TABLE 3-10. COST PROJECTIONS FOR TWO FUNDAMENTAL DESIGNS OF ESB MODULES

System Component	Integral (ESB) Front Conventional Back		Integral (ESB) Front Glass (ESB) Back	
	Material	\$/m <sup>2</sup>	Material	\$/m <sup>2</sup>
Front Glass	7070	3.22 <sup>1</sup>	7070	3.22 <sup>1</sup>
Back Laminating Compound	EVA	0.47 <sup>2</sup>	Inorganic interface	0.25
Back Cover (Moisture Barrier and Electrical Insulation)	Al/Mylar	0.71	7070 glass	3.22
<b>TOTALS</b>				
	\$/m <sup>2</sup>	4.40		6.69
	\$/W <sub>pk</sub> @ 13% AM1 module efficiency	0.034		0.051

1. Based on Corning Glass Works projection of April 1978.
2. Springborn Laboratory estimate of December 1979 presented at 11th LSA Project Integration Meeting.

### 3.10 FUTURE DEVELOPMENT OF INTEGRAL GLASS ENCAPSULATION

Phase I of this program identified electrostatic bonding as a technically excellent process for terrestrial solar cell encapsulation. Environmental tests showed that potential for achieving a 20-year life encapsulation system was high. Phase II provided more evidence of stability of ESB systems and demonstrated practical configurations in which all module components were included.

Phase III will concentrate on demonstration of the production readiness of integral glass encapsulation by electrostatic bonding. Both the integral front/conventional back (Type I) and all glass (Type II) modules will be produced in quantity.

Module size will be consistent with the LSA minimodule design. However, since present electrostatic bonding equipment is not large enough to process samples of the required size, minimodules will be assembled from four ESB modules. The cell layout for these modules is shown in Figure 3-35.

Additional minimodules will be fabricated in sufficient quantity to demonstrate advanced development concepts such as preformed wire mesh contacts. Demonstration of a high efficiency module, employing the best available technology, will be a part of the development efforts.

An additional task of Phase III will be to develop preliminary plans for a large-area electrostatic bonder. Efforts during Phase III will address the problems of size scaleup. It is expected that these plans, coupled with the demonstration of routine fabrication of ESB modules, will justify the construction of a full-scale bonder capable of producing practical sized, field usable solar modules.

## SECTION 4

### CONCLUSIONS

This program has advanced integral glass encapsulation to the point at which practical solar module designs have been demonstrated. Phase I showed that electrostatic bonding could be used as an encapsulation technique and that the resulting demonstration modules were superior in their resistance to environmental effects. During Phase II the module concepts of Phase I were refined into practical demonstration structures. These advances in module design and sophistication were accomplished through a variety of equipment and process improvements. Major accomplishments of Phase II of this program include:

- Addition of total microprocessor control of all bonding functions.
- Addition of real-time monitoring and displaying of bonding parameters.
- Introduction of a batch loading capability allowing the processing of five samples without breaking the bonding environment.
- Addition of pre-/post-bond heating of samples to speed processing and provide annealing of bonded samples.
- Evaluation of glass materials developed especially for electrostatic bonding and identification of two alternate glasses (in addition to Corning 7070) that could be used for this process.
- Definition of a development plan that will result in a glass production process yielding low cost borosilicate glass. Ultimately, borosilicate glass can be nearly as inexpensive as soda lime glass.
- Demonstration of practical module configurations which include high cell packing density (>90 percent), output terminals that maintain module hermeticity, and low cost module backings.
- Identification of production processes and sequences for module fabrication.
- Broadening of the range of demonstrated bondable forms of silicon to include ribbon, cast polycrystalline, and texture etched in addition to polished and bright etched Czochralski and float-zone wafers.

- Identification, through bond quality measurement, of acceptable ranges of bond parameters.
- Demonstration of advanced metallization concepts including preformed wire mesh contact and screen-printed contacts on glass.
- Additional accelerated environmental test results show no degradation in encapsulated cell electrical performance or mechanical integrity. These positive results are additional evidence of the superior performance of integral glass encapsulation and that electrostatically bonded solar modules should have lifetimes of at least 20 years.
- Realistic cost estimates for ESB encapsulation systems have been prepared and the costs are consistent with LSA Project goals.

## REFERENCES

1. Handbook of Chemistry and Physics, 57th Edition, CRC Press, Cleveland, Ohio (1976), pp. B85-178 and E219.
2. "Low Temperature Fabrication of High Efficiency Silicon Solar Cells", AFAPL Technical Report No. AFAPL-TR-77-86, Spire Corporation, Bedford, Massachusetts (1978), pp. 57-60.
3. "High Efficiency Solar Panel", AFAPL Technical Report No. AFAPL-TR-77-36, Spectrolab, Inc., Sylmar, California (1977), pp. 52-55.
4. "High Output Solar Cell with Multilayer AR Coating", AFAPL Technical Report No. AFAPL-TR-77-71, Optical Coating Laboratory, Inc., City of Industry, California (1977).
5. Spire measurements (unpublished).
6. "Integral Glass Encapsulation for Solar Arrays", JPL/DOE Contract No. 954521, Interim Report No. 1, Spire Corporation, Bedford, Massachusetts (1977), pp. 44-53.
7. "Project Quarterly Report-5", Department of Energy LSSA Project DOE/JPL-1012-77/4, JPL Publication 78-9, LSSA Document 5101-46, Jet Propulsion Laboratory, Pasadena, California (1978).